Taylor & Francis
Taylor & Francis Group

Dealing with homoplasy: osteology and phylogenetic relationships of the bizarre neobatrachian frog Baurubatrachus pricei from the Upper Cretaceous of Brazil

Ana María Báez & Raúl Orencio Gómez

🗎➕ View supplementary material 🗗

📅 Published online: 28 Feb 2017.

🖉 Submit your article to this journal 🗗

🔍 View related articles 🗗

CrossMark View Crossmark data 🗗

Taylor & Francis
Taylor & Francis Group

Dealing with homoplasy: osteology and phylogenetic relationships of the bizarre neobatrachian frog *Baurubatrachus pricei* from the Upper Cretaceous of Brazil

Ana María Báez[a,b]* and Raúl Orencio Gómez[a]

[a]CONICET-IGEBA-Departamento de Ciencias Geológicas, Facultad de Ciencias Exactas y Naturales, Universidad de Buenos Aires, Ciudad Universitaria, Buenos Aires, Argentina; [b]Museo Argentino de Ciencias Naturales 'Bernardino Rivadavia', Buenos Aires, Argentina

The hyperossified frog *Baurubatrachus pricei* Báez & Peri 1989 from the Maastrichtian Serra da Galga Member of the Marília Formation is described in detail, as preparation of the type and only known specimen revealed significant features, particularly of the pectoral and pelvic girdles. This species is rediagnosed on the basis of the combination of plesiomorphic and derived character states, including two unique traits: cranial roof with round openings that might have contained the tympanic membrane completely circumscribed by ornamented dermal bone, and scapula bearing a conspicuous crest deflected ventrally to form a deep basin on its leading edge. Since its discovery it was suggested that *Baurubatrachus* might be a relative of the South American ceratophryids, a phylogenetic placement endorsed by recent analyses. In order to test this hypothesis considering all the available information, we conducted several maximum parsimony analyses under different weighting schemes and topological constraints, scoring 143 characters for 71 extant and extinct anuran taxa. Our taxonomic sampling included species with well-ossified dermatocrania as well as less ossified members of main neobatrachian clades to explore the impact of hyperossification, which frequently drives groupings based on homoplastic features. We also assessed the phylogenetic signal provided by cranial and postcranial partitions. Although we recovered a monophyletic Ceratophryidae repeatedly, *Baurubatrachus* was not related with this nobleobatrachian group but associated with the calyptocephalellid australobatrachians, although with weak support. Other possible phylogenetic placements are also discussed, as well as microhabitat and habits, taking into account both anatomical and geological data.

Keywords: Neobatrachia; Ceratophryidae; Australobatrachia; South America; Maastrichtian; phylogeny

Introduction

Anurans are a relatively morphologically homogeneous group when compared with other tetrapods, although distinctive morphotypes that may be found in similar but distant habitats have evolved repeatedly along their history. Instances of substantial morphological similarity in frogs as well as in other groups of vertebrates and the responsible underlying mechanisms have long been a central issue in evolutionary biology (e.g. Moen *et al.* 2013, 2016; Darda & Wake 2015; Wake *et al.* 2015, and citations therein). The recurrent appearance of sets of traits in members of lineages phylogenetically distant based on molecular evidence usually blurs their relatedness and it is obvious that the similarity not inherited from a common ancestor constitutes a hindrance to the development of phylogenetic hypotheses based on morphological data and to the placement of fossil taxa, such as the one discussed herein.

Báez and Perí (1989) briefly described the partially articulated, nearly complete, well-ossified skeleton of a frog three-dimensionally preserved in two pieces of coarse sandstone (DNPM Paleontologia 1412-R A and B). The specimen was collected in 1969 by Llewelyn Ivor Price and Diogenes de Almeida Campos near Uberaba in the Triângulo Mineiro region, Minas Gerais State, mid-south-eastern Brazil (Fig. 1), from conglomeradic sandstone of the Serra da Galga Member of the Marília Formation (Báez 1985). The latter formation is the uppermost unit of the continental Late Cretaceous Bauru Group, which was deposited in the Bauru Basin subsequent to the rifting phase related to the break-up between Africa and South America (Fernandes & Coimbra 2000) and is well known for its abundant vertebrate fossil content (e.g. Goldberg & Garcia 2000). Some exposures of the Serra da Galga Member in the Uberaba region include facies representing alluvial fans and ephemeral braided fluvial systems deposited under a semiarid climate with marked seasonality (Fernandes 2010).

Báez & Perí (1989) considered that DNPM Paleontologia 1412-R A and B (Fig. 2A–C) represents a new neobatrachian, *Baurubatrachus pricei*, which might be related to the

---

*Corresponding author. Email: baez@gl.fcen.uba.ar
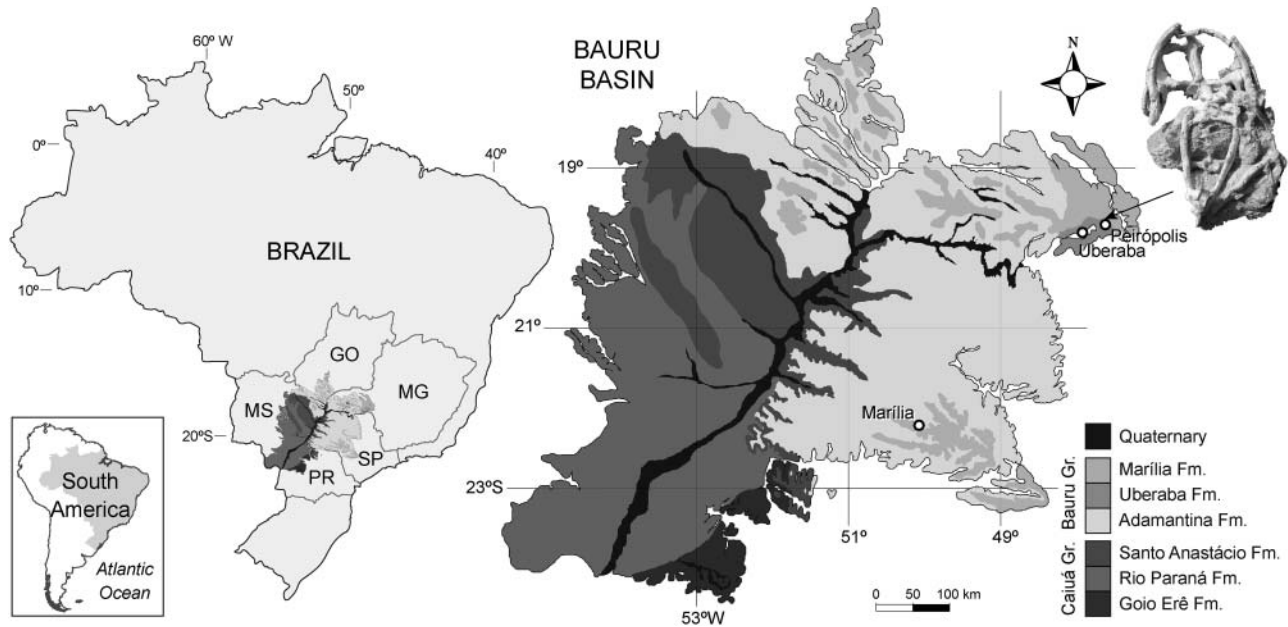
Figure 1. Map of Brazil, showing the location of the Bauru Basin and the fossil site where the remains of *Baurubatrachus pricei* (DNPM Pal. 1412-R A, B) were discovered.

clade formed by the extant Neotropical hyperossified frogs *Ceratophrys*, *Chacophrys* and *Lepidobatrachus* (Ceratophryini *sensu* Frost *et al.* 2006 or Ceratophryidae *sensu* Pyron & Wiens 2011; Frost 2014). Notwithstanding, Báez & Perí (1989) acknowledged the presence of many features unknown in the living members of this distinctive anuran group and suggested that the resemblance also might be the result of convergent evolution (Báez & Peri 1989).

Subsequently, several morphology-based phylogenetic analyses or analyses using morphological and molecular characters in combination (Evans *et al.* 2008, 2014; Ruane *et al.* 2011; Laloy *et al.* 2013) included *Baurubatrachus* in their datasets, retrieving a position for this taxon either within crown Ceratophryidae or as a member of its stem. However, thorough discussions of these results have not been provided, probably because the placement of this Cretaceous taxon was not the main focus of these studies. Further preparation of the material revealed additional characters, mainly of the pectoral girdle, forelimb, and pelvis as discussed below, which call into question its relationship with ceratophryids. This information prompts a more detailed description, as well as the reassessment of the relationships of this frog (Báez *et al.* 2005; Báez & Gómez 2014). In addition, recent proposals of neobatrachian relationships based mainly on DNA sequence data (e.g. Frost *et al.* 2006; Pyron & Wiens 2011; Zhang *et al.* 2013) have changed the phylogenetic context in which a discussion of the placement of *Baurubatrachus* should be conducted, although the lack of a robust phylogenetic hypothesis based on morphological synapomorphies makes it difficult to evaluate its taxonomic position.

Therefore, a careful evaluation of all available morphological evidence that supports the taxonomic position of *Baurubatrachus* seems relevant, especially considering the use of this taxon as one of the calibration points for constructing a molecular time-scale of the major diversification of crown-group Anura (e.g. Roelants *et al.* 2007). Herein we redescribe the skeleton of *Baurubatrachus*, including new features exposed by the preparation of the holotype. We also test the evolutionary relationships retrieved in recent studies and evaluate the impact of features linked to hyperossification on the reconstruction of its affinities on the basis of osteological characters by performing parsimony analyses, taking into account all the available evidence.

Material and methods

Institutional abbreviations
AMNH: American Museum of Natural History, New York, USA; **DNPM**: Direção Nacional da Produção Mineral, Seção Paleontologia, Rio de Janeiro, Brazil; **FCEN**: Facultad de Ciencias Exactas y Naturales de la Universidad de Buenos Aires, Buenos Aires, Argentina; **FML**: Instituto de Herpetología de la Fundación Miguel Lillo, Tucumán, Argentina; **FMNH**: The Field Museum, Chicago, USA; **MNCN**: Museo Nacional de Ciencias Naturales, Madrid, Spain; **MNHN**: Muséum national d'Histoire naturelle, Paris, France; **KU**: Natural History Museum, University of Kansas, Lawrence, USA; **MACN**: Museo Argentino de Ciencias Naturales 'Bernardino
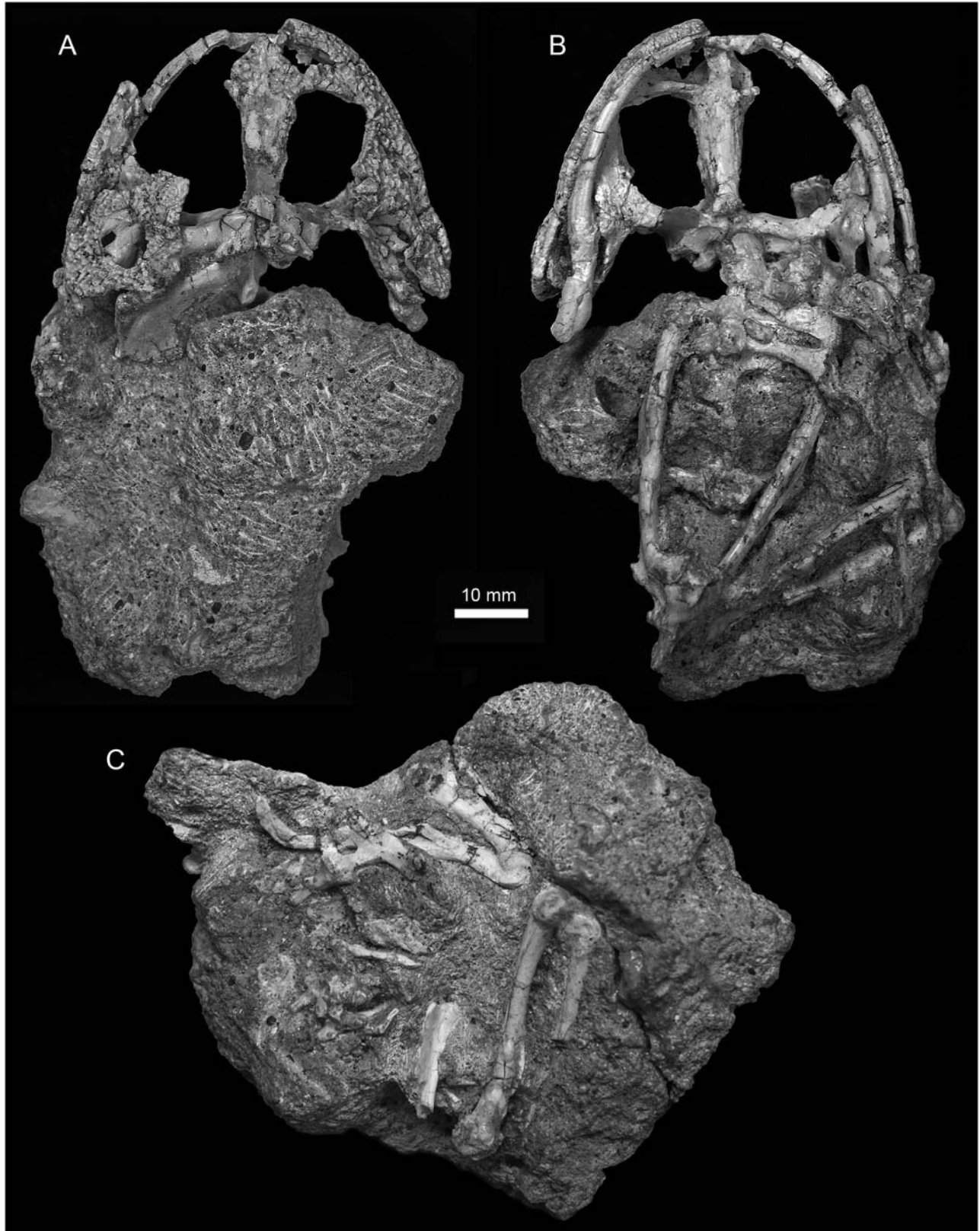
Figure 2. *Baurubatrachus pricei*, holotype. **A,** DNPM Pal. 1412-R B, skull and partial postcranium in dorsal aspect; **B,** DNPM Pal. 1412-R B, skull and most of the postcranium in ventral aspect; **C,** DNPM Pal. 1412-R A, partial postcranium in dorsal aspect.

Rivadavia', Buenos Aires, Argentina; **MCN**: Museo de Ciencias Naturales de la Universidad Nacional de Salta, Salta, Argentina; **MCZ**: Museum of Comparative Zoology, Harvard University, Cambridge, USA; **MPEF**: Museo Paleontológico Egidio Feruglio, Trelew, Argentina; **MSUVP**: Michigan State University Museum, East Lansing, USA.

Specimen description

The studied specimen was originally preserved in two pieces of sandstone: DNPM Pal. 1412-R A and B. Part of the skull as well as elements of the postcranial skeleton were preserved in block A (Fig. 2C); subsequently, this portion of the skull was glued to the portion of the skull preserved in block B, in order to restore the entire cranial architecture, which now is exposed dorsally and ventrally (Fig. 2A, B). Later on, the pelvic girdle lying on block B was carefully prepared mechanically under the microscope, exposing the acetabular view of the right ilium and ischium as well as the distal portion of the right sacral diapophysis.

General osteological terminology used in this paper mostly follows that of Bolkay (1919), Trueb (1973) and Roček (2003); terminology concerning carpal and tarsal elements is that of Fabrezi & Alberch (1996) and Fabrezi (1992, 1993) and that of the ilium follows Gómez & Turazzini (2016). The taxonomy follows that of Frost (2014), unless stated otherwise. Illustrations were prepared with the aid of a Nikon SMZ 1000 microscope with a camera lucida attachment. Photographs were made using a Nikon D3200 digital camera equipped with a macro lens. Measurements were taken with a dial calliper to the nearest 0.1 mm.

Phylogenetic analyses

Based on the previous hypotheses on the relationships of *Baurubatrachus* noted above, our taxon sampling, presented in the Supplemental material, focused on neobatrachians representing major Hyloides lineages, in particular extant members of earliest branching lineages according to recent broad-scale phylogenetic analyses (e.g. Frost *et al.* 2006; Pyron & Wiens 2011). Whenever possible, we selected taxa with well-ossified dermatocrania as well as less-ossified relatives to test the influence of dermal hyperossification and included taxa that were part of the dataset in previous studies. We scored several representatives of the three genera currently included in Ceratophryidae to consider variation within this clade. We also included exemplars of several species of telmatobiids in view of the close relationship of the latter with ceratophryids retrieved in some analyses (Frost *et al.* 2006; Pyron & Wiens 2011; Blotto *et al.* 2013; Zhang *et al.* 2013, but see Gomez-Mestre *et al.* 2012) and the

substantial intrageneric osteological variation in *Telmatobius* (De la Riva *et al.* 2012). Representatives of other groups supposedly closely related to ceratophryids, such as odontophrynids (Fabrezi & Quinzio 2008), were also considered. In addition, ingroup taxa also included some extinct neobatrachian taxa, such as the Cretaceous putative ceratophryid *Beelzebufo ampinga* from Madagascar (Evans *et al.* 2008, 2014) and *Cratia gracilis*, *Arariphrynus placidoi* and *Eurycephalella alcinae* from the mid Cretaceous of north-eastern Brazil (Báez *et al.* 2009), as well as the Eocene *Thaumastosaurus gezei* from France, formerly considered close to South American hyloids and now a ranoid (Laloy *et al.* 2013). We excluded the putative Miocene Patagonian ceratophryid *Wawelia* from the analysis because the only known specimen belongs to an immature individual and is poorly preserved (Báez & Perí 1990; Nicoli *et al.* 2016); therefore, its identification is doubtful. In addition, we sampled several representatives of non-neobatrachian frogs.

In total, 71 extant and extinct species were scored for 143 morphological characters (62 cranial, 12 of the hyobranchial skeleton, 68 postcranial, and one of the soft-tissue anatomy), most of which have been used in previous analyses (e.g. Fabrezi 2006; Scott 2005; Báez *et al.* 2009, 2012; Henrici *et al.* 2013; and papers cited therein). Definitions of many characters have been rephrased following the suggestions made by Sereno (2007) to make their meanings explicit. In order to describe the morphological variation of the taxonomic sample more accurately, some characters include more states than in previous studies. This is indicated in the complete character list and additional comments, both included in the Supplemental material. The matrix, presented in the Supplemental material, was constructed using Mesquite v2.75. Some taxa were rescored either because more or better-preserved specimens were available to us or were miscoded in previous analyses according to recent published information (Supplemental material). All analyses (full matrix with characters equally weighted, those multistate considered as unordered and as ordered; the putative hyperossification-linked characters removed, all cranial characters removed, all postcranial characters removed; constrained searches) were run with TNT v. 1.5-beta (Goloboff *et al.* 2008). In all instances the heuristic search with 1000 replicates of Wagner trees and a random addition sequence of taxa, followed by tree bisection reconnection (TBR) branch swapping, holding ten trees per replication, was used. The resulting trees were subjected to a final round of TBR branch swapping and the final trees were rooted with *Ascaphus truei*.

Unconstrained analyses with unordered multistate characters and characters subjected to implied weighting with integer values of the concavity constant k = (1–30) were performed to assess sensitivity of the results to variations of the strength of the weighting function. Constrained

analyses with unordered multistate characters were also performed both under equal weights and implied weights (k = 7), forcing *Baurubatrachus* within Ceratophryidae in one analysis and using the topologies of Pyron & Wiens (2011) for Anura and of Faivovich *et al.* (2014) for Ceratophryidae, with fossil taxa as floating terminals, in another. Node support was expressed using absolute frequencies under jackknifing with 10,000 pseudo-replicates and the Bremer index.

Systematic palaeontology

Anura Fischer von Waldheim, 1813
Neobatrachia Reig, 1958
Genus *Baurubatrachus* Báez & Perí, 1989

Type species. *Baurubatrachus pricei* Báez & Perí, 1989.

Baurubatrachus pricei Báez & Perí 1989
(Figs 2–6, 7A, B)

Holotype. DNPM Pal. 1412-R A and B, an incomplete, partially articulated skeleton preserved within two pieces of sandstone, lacking part of the skull and anterior and posterior autopodia (Fig. 2A–C).

Type locality. BR262 route (Uberaba-Belo Horizonte), 3.3 km north-east of Peirópolis, Uberaba District, Minas Gerais State, mid-south-eastern Brazil (Fig. 1).

Type horizon and age. Serra da Galga Member, Marília Formation, Bauru Group, Maastrichtian (Late Cretaceous).

Revised diagnosis. Neobatrachian frog diagnosed by the combination of the following character states (autapomorphies marked with an asterisk): large size; heavily ossified skeleton with a moderately depressed skull; dermal roofing skull bones bearing sculpture consisting of tubercles and rounded pits that nearly reach the ventral margin of the maxillary arcade; high *pars facialis* throughout the length of the maxilla; nasals in broad contact with one another along the midline; discrete triangular palatines (neopalatines of Trueb (1993)) tapering medially and well separated medially from one another; massive pterygoid with anterior ramus bearing a conspicuous ventral flange* and medial ramus broadly sutured with the corresponding parasphenoid ala, parasphenoid alae lacking ventral keels; squamosal having an extensive *lamella alaris* in contact with the maxilla anteriorly and laterally forming at least part of the border of a round opening that might have contained the tympanic membrane and is completely surrounded by dermal bone; extensive sphenethmoidal ossification extending into the *septum nasi* anteriorly* and the *planum antorbitale* laterally* and roofing the *cavum cranii* posteriorly, lower jaw articulation well posterior to the occiput, eight discrete presacral vertebrae, high

atlantal neural spine partially fused to succeeding neural arch, transverse processes of Vertebrae III and IV expanded distally and reaching farther laterally than the moderately expanded sacral diapophyses, moderately long scapula bearing a conspicuous crest deflected ventrally to form a deep basin on its leading edge, well-ossified, large cleithrum with anterior branch and plate-like posterior portion; robust clavicle strongly bowed anteriorly; ilium with well-developed dorsal crest and an elongate dorsal protuberance obliquely oriented and strongly projected laterally but barely projecting from iliac outline in acetabular view*; ventral acetabular expansion and iliac shaft forming an angle of nearly 70°*; ischium bearing a large posterodorsal expansion; pubis at least partially ossified; femur bearing a crest.

Anatomical description

Preservational and general anatomical aspects

The skeleton is partially articulated; the skull is somewhat dorsoventrally crushed and components of the hyoid and middle ear apparatuses as well as autopodia of fore- and hind limbs are not preserved. The snout–vent length (SVL) is estimated to have been about 110 mm, although it should be noted that the sacral diapophyses are preserved at mid-length of the iliac shafts indicating some postmortem fore-aft sliding of the latter skeletal elements. The axial skeleton is incomplete; some of the posterior presacral vertebrae are disarticulated and preserved in different aspects, although they are located near their natural positions. Only the most anterior portion of the urostyle is preserved. The marked sculpturing of the roofing bones of the skull and the general high degree of ossification of the entire skeleton clearly indicate that DNPM Pal. 1412-R belongs to an adult individual.

Exocranium

Most dermal roofing bones have broad contacts to one another; this extension of the dermal bones confers a massive appearance to the skull, which is roughly triangular in dorsal view and moderately depressed (Figs 3A, B, 4A). Despite this extensive deposition of bone, crests are not evident on the skull roof. The maximum width of the skull, which is coincident with the level of the lower jaw articulation, is about 1.30 times the median length, measured from the anterior margin of the skull, roughly estimated owing to the lack of preservation of the premaxillae, to the posterior margin of the occipital condyles. All preserved roofing bones bear dermal ornamentation; this ornamentation is very irregular and differs in different parts of the skull (Figs 3A, 4A, C, D). In general, it consists of large, deep, rounded pits that are smaller and shallower along the orbital and
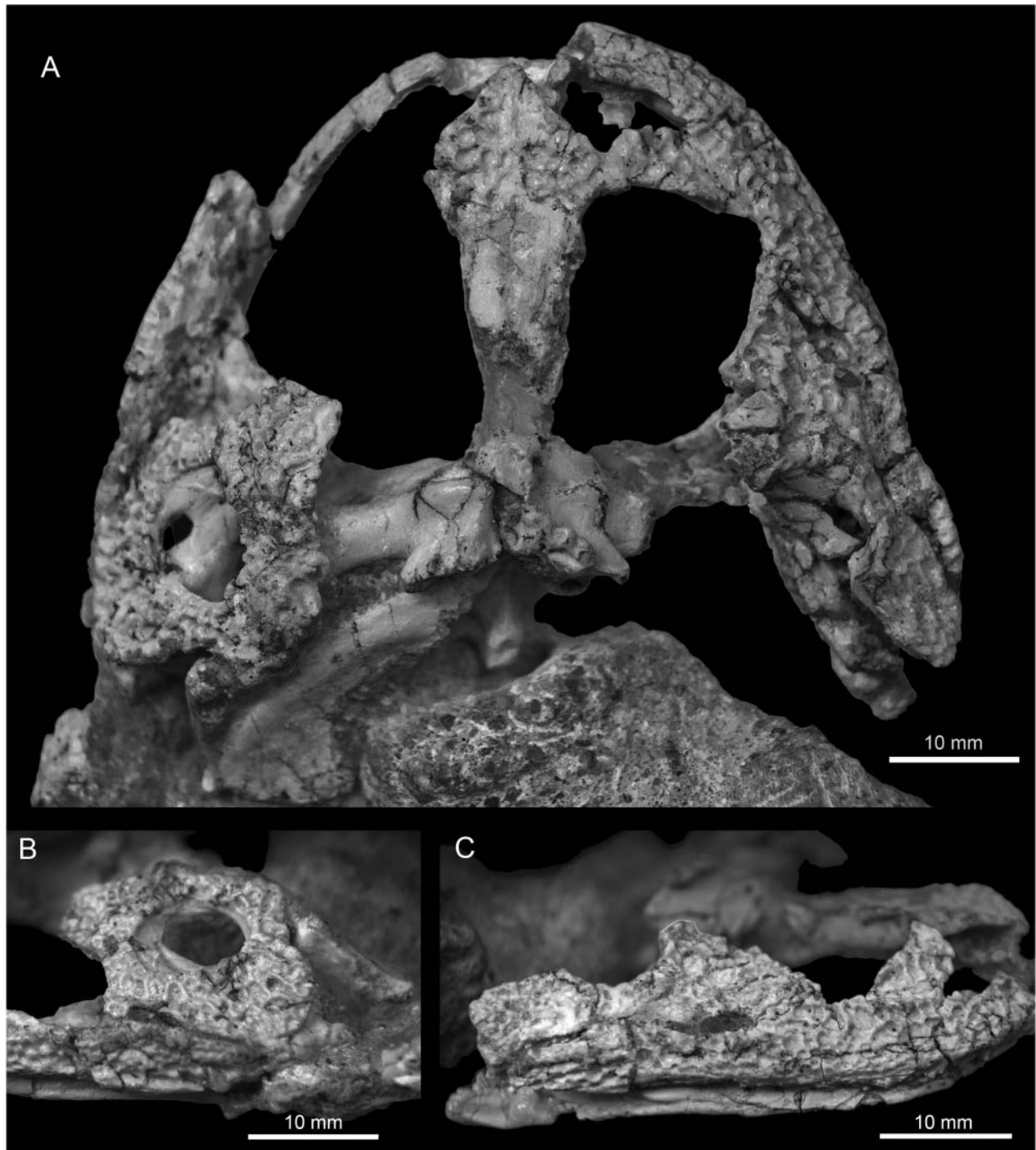
Figure 3. *Baurubatrachus pricei*, holotype (DNPM Pal. 1412-R B). **A,** skull in dorsal view; **B,** close-up of the temporal region in dorso-lateral view; **C,** close-up of the right maxilla in lateral view.

narial margins of the nasals as well as surrounding the tympanic openings. Some parts of the exocranium, such as the *lamella alaris* of the squamosals, also bear rounded tubercles that in some areas seem to have fused to form moniliform ridges delimiting irregular channels. The lack of sutures owing to hyperossification and bone fusion, and, perhaps, ossification of the dermis make it difficult the interpretation of the boundaries and relationships of the individual bones of the skull. The median length of the preorbital region represents nearly 40% of the maximum median length of the skull. The lower jaw joint is located well posterior to the occiput.
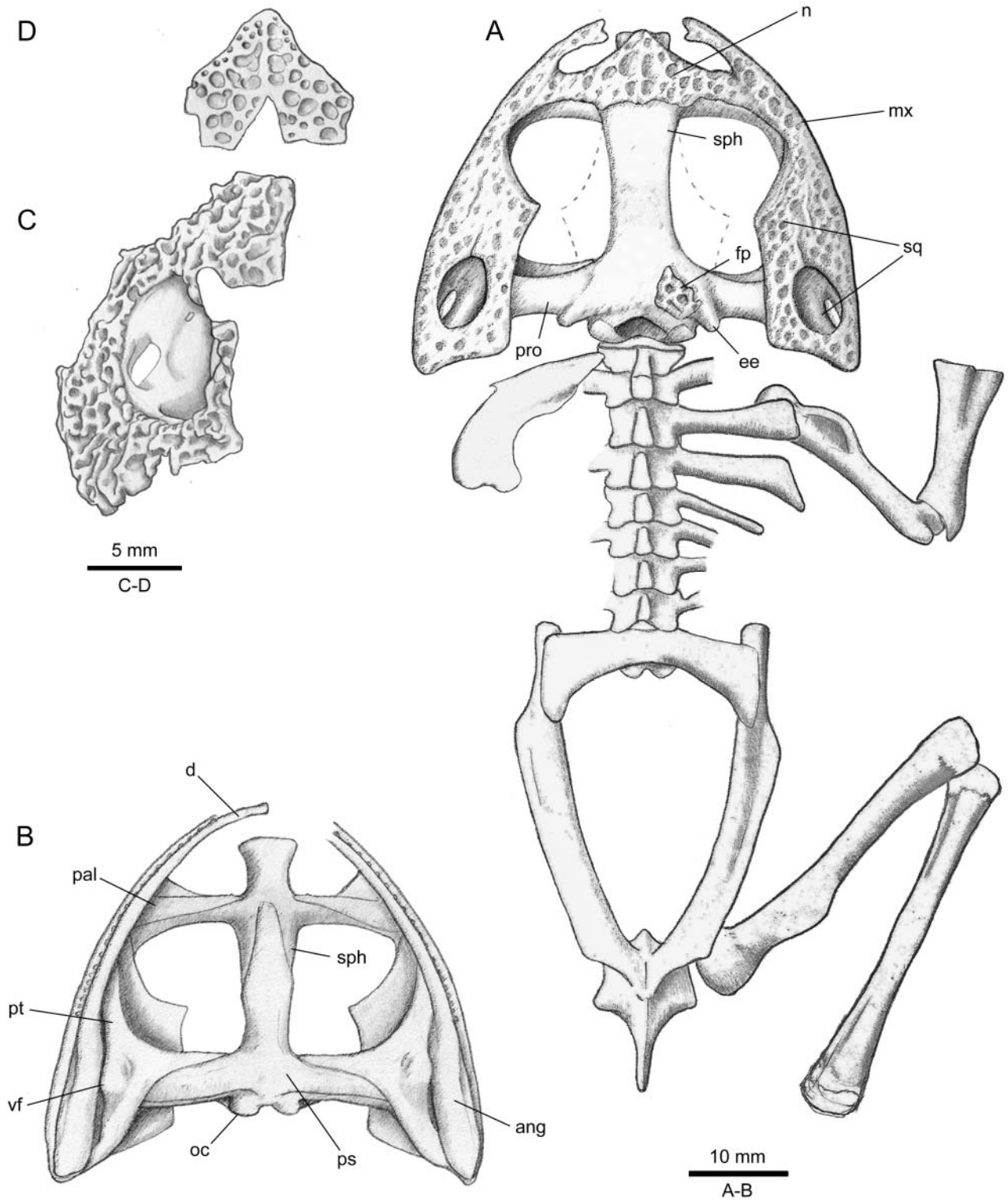
Figure 4. *Baurubatrachus pricei*, holotype (DNPM Pal. 1412-R). **A,** restoration of partial skeleton in dorsal aspect; **B,** restoration of the skull in ventral aspect; **C,** detail of the squamosal ornamentation; **D,** detail of the nasal ornamentation. Abbreviations: ang, angulosplenial; d, dentary; ee, epiotic eminence; fp, frontoparietal; mx, maxilla; n, nasal; oc, occipital condyle; pal, palatine; pro, prootic; ps, parasphenoid; pt, pterygoid; sph, sphenethmoid; sq, squamosal; vf, ventral flange. Dashed lines indicate the lateral extent of the frontoparietals.
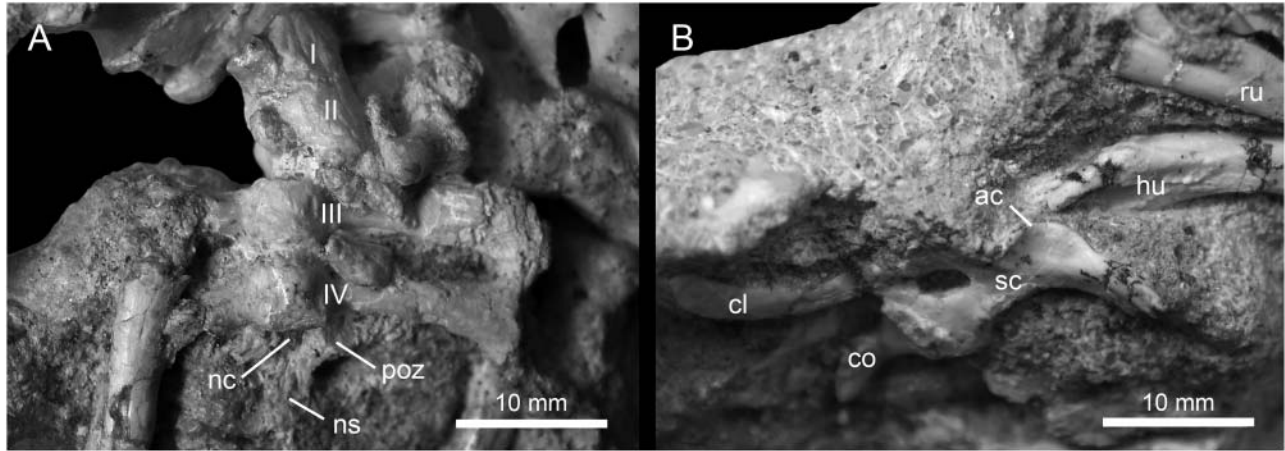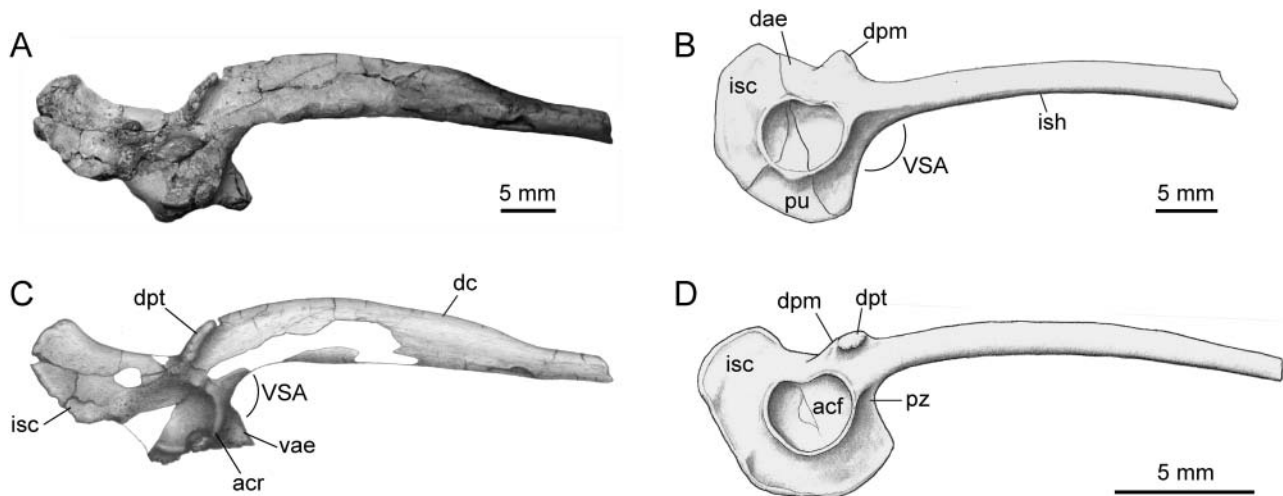
Figure 5. *Baurubatrachus pricei,* holotype (DNPM Pal. 1412-R). **A,** close-up of the anterior presacral vertebrae in ventral aspect; **B,** close-up of the elements of the pectoral girdle in dorsal aspect. Abbreviations: ac, anterior crest of scapula; cl, clavicle; co, coracoid; hu, humerus; nc, neural canal; ns, neural spine; poz, postzygapophysis; ru, radioulna; roman numerals I–IV: presacral vertebrae; sc, scapula.
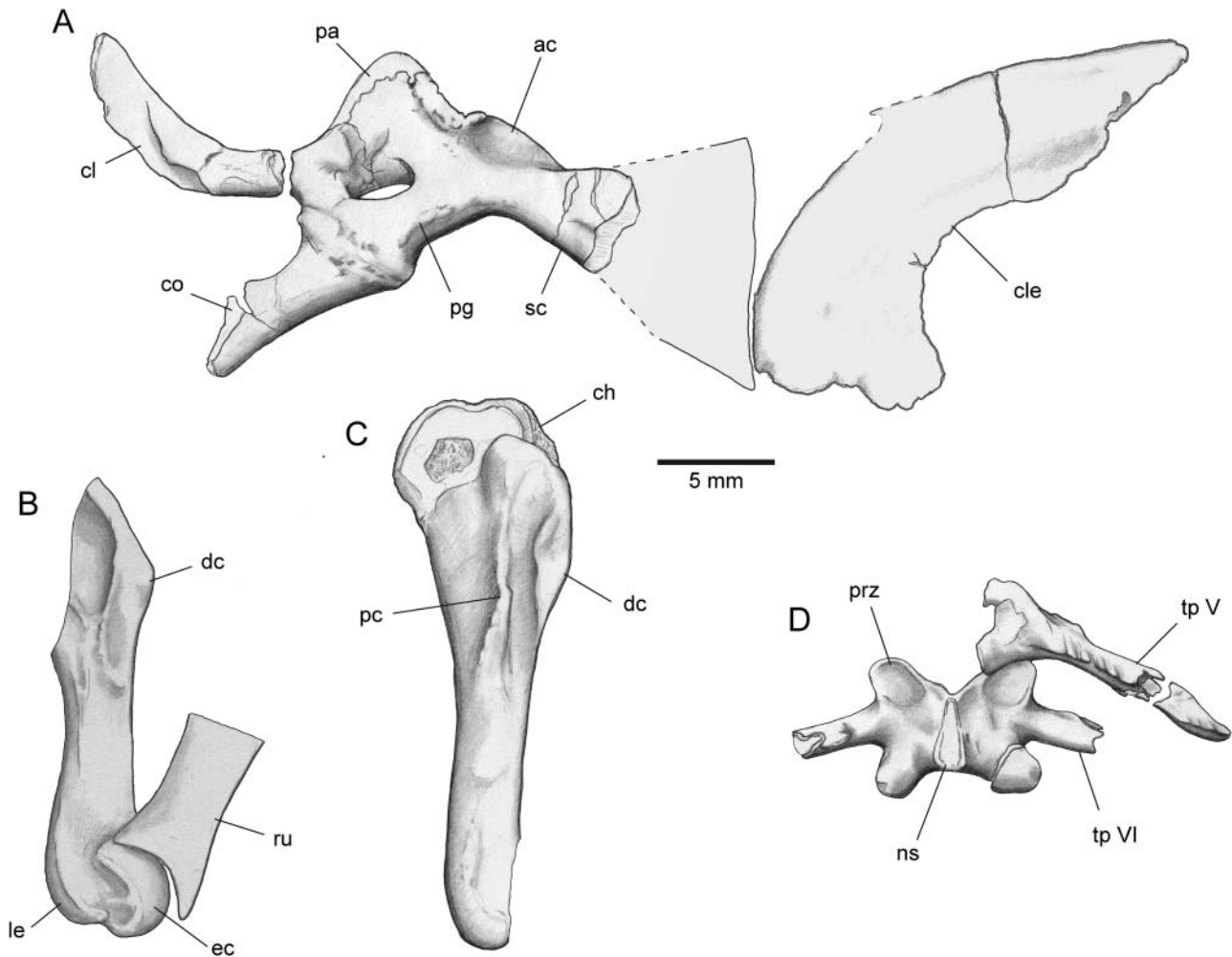
Figure 6. *Baurubatrachus pricei,* holotype (DNPM Pal. 1412-R), interpretive drawings of selected postcranial elements. **A,** partial right half of pectoral girdle in dorsal view; **B,** DNPM Pal. 1412- R A, right humerus in lateral view; **C,** DNPM Pal. 1412-R B, left humerus in ventromedial view; **D,** vertebrae V and VI in dorsal view. Abbreviations: ac, anterior crest of scapula; ch, *caput humeri*; cl, clavicle; co, coracoid; cle, cleithrum; dc, deltoid crest; ec, *eminentia capitata*; le, lateral epicondyle; ns, neural spine; pa, *pars acromialis*; pg, *pars glenoidalis*; pc, parietal crest; prz, prezygapophysis; ru, radioulna; sc, scapula; tp, transverse process. Dashed lines indicate the reconstructed bone margins based on anatomical continuity and/or impressions.

Figure 7. *Baurubatrachus pricei* holotype (DNPM Pal. 1412-R B). **A,** photograph of pelvic girdle in right lateral view; **B,** interpretive drawing of A; **C,** pelvic girdle of *Lepidobatrachus laevis* FCEN 319 in right lateral view; **D,** pelvic girdle of *Telmatobius scrochii* FML 1515 in right lateral view. Abbreviations: acf, acetabular fossa; acr, acetabular rim; dae, dorsal acetabular expansion; dc, dorsal crest; dpm, dorsal prominence; dpt, dorsal protuberance; isc, ischium; ish, iliac shaft; pz, preacetabular zone; pu, pubis; vae, ventral acetabular expansion; VSA, angle between the ventral acetabular expansion anterior margin and the iliac shaft.

Nasals. These paired dermal bones are in contact to one another along their medial margins; a distinct suture is not present but the area of contact between the contralateral elements is discernible by the discontinuous ornamentation (Figs 3A, 4A, D). The nasals are co-ossified with the underlying ossified *tectum nasi*, anteriorly, and sphenethmoid, posteriorly. Each nasal has an anteriorly tapering, short rostral process and extends laterally to form a well-developed maxillary process that is fused posteriorly to the ossified postnasal wall. The maxillary process has a long axis nearly perpendicular to the midline of the skull, whereas its distal end is anteroposteriorly expanded and in contact with the dorsal margin of the *pars facialis* of the corresponding maxilla. Anteriorly, the nasal forms the posterolateral border of the ample fenestra exonarina, whereas posteriorly it forms the anterior margin of the orbit. At the anterolateral angle of the orbit, however, the most posterior portion of the maxillary process is slightly broken and thus it is difficult to assess whether this bone contacted the dermal element that forms the lateral margin of the orbit. At the anteromedial corner of the orbits, the nasals are in contact with a few remnants of the frontoparietals that lie on the right side of the roof of the braincase.

Frontoparietals. These bones are largely missing; consequently, it is difficult to reconstruct their shape and extent. Fragments of ornamented dermal bone that we interpret as part of the right frontoparietal are preserved fused to the sphenethmoid, anteriorly, and to the prootic, posteriorly (Figs 3A, 4A). The most anterior putative preserved fragment of the frontoparietal is fused to the dorsal surface of the sphenethmoid and extends from the right nasal to the level of the reconstructed posterior margin of the orbit. Also, an elongate portion of ornamented bone that we consider part of the frontoparietal was preserved, forming the posteromedial margin of the right orbit (Báez & Perí 1989, p. 451, fig. 4A), but it was lost during the subsequent preparation of the specimen. This latter formerly preserved portion of the frontoparietal provided evidence for the presence of a supraorbital flange (*tectum supraorbitale* of Roček 2003) but it was not large enough to reconstruct the entire outline of the bone. Ventrolaterally, the extent of the *pars contacta* or *lamina perpendicularis* cannot be determined owing to its complete fusion with the lateral wall of the sphenethmoid. Posteriorly, on the right side, a portion of heavily sculptured dermal bone is fused to the anterior two-thirds of one of the two prominent parasagittal crests formed by the prootic bones; each of these crests probably corresponds to the prominence of the *ductus semicircularis posterior* (= epiotic eminence), suggesting that the frontoparietal did not rest flat on the dorsal surface of the otic capsule. No smooth lateral flange (otic flange) developed by the frontoparietal is discernible on the dorsal wall of the otic capsule. Posteromedially, the frontoparietal terminates near the level of the dorsal margin of the foramen magnum according to the preserved small piece of this bone near the right occipital condyle (Fig. 4A). On the occiput, at the level of the right occipital condyle and ventral to the ornamented surface of the frontoparietal, there is a foramen for the occipital artery, which in life was contained within a channel roofed by the frontoparietal.

Maxillary arch. The premaxillae are missing. The right maxilla is almost entirely preserved (Fig. 3A), whereas only the posterior half of the left maxilla is represented.

The anterior margin of the high *pars facialis* of the maxilla is slightly concave; no anterodorsal process (see Supplemental Fig. S4) formed by the *pars facialis* of the maxilla is evident. The ornamentation on the external surface of the *pars facialis* reaches the *pars dentalis* (Fig. 3C). Although dorsoventral crushing of the skull has produced some deformation of the maxillary arch, a protruding band of bone along the *pars dentalis* is not evident (see Supplemental Fig. S4 and character 50 in the Supplemental material). A depressed area along the contact between the maxillary process of the nasal and the *pars facialis* of the maxilla marks the path of the nasolachrimal duct. Posterior to this area, the maxilla is slightly broken so it cannot be determined with certainty whether the bone that clearly forms part of the concave lateral orbital margin is part of the maxilla; farther posteriorly, the maxilla articulates with the extensive *lamella alaris* of the squamosal. The maxillary arch extends posteriorly to near the *pars articularis* of the quadrate; a quadratojugal pars jugalis joining the posterior process of the maxilla to the *pars articularis* of the quadrate is probably present but there are no traces of sutures owing to the high degree of coalescence of these bones. A few fine, elongate wrinkle-like ridges occur along the ventral margin of the maxilla in the region that probably corresponds to the posterior process of this bone. However, an ornamented dorsal flange that is anteriorly continuous with the maxillary *pars facialis* extends posteriorly along this region up to the end of the maxillary arch close to the level of the lower jaw articulation. On both sides of the skull an oblique crack separates this dorsal flange from the *lamella alaris* of the squamosal (Fig. 3B, C). Although these right and left cracks probably are postmortem artefacts owing to some dorsoventral depression of the skull, they might indicate lines of weakness along a former contact between the respective maxillary arches and squamosals. The quadratojugal may have been dorsally expanded to form a flange analogous to the maxillary *pars facialis* or the maxilla may have extended posteriorly with a reduced quadratojugal bracing this bone against the posterior end of the palatoquadrate; in any case, it is evident that the subtemporal fenestra was probably reduced or absent altogether, as suggested previously (Báez et al. 2005).

The maxilla bears a distinct palatine shelf (*pars palatina*), although the most anterior portion of this shelf is not preserved and, hence, we were unable to describe the configuration of the articulation with the premaxilla in detail. The *pars palatina* is well developed and its lingual margin has a rounded cross section along its anterior part up to near the level of the anterior margin of the orbit, whereas more posteriorly it is slightly dorsoventrally flattened against the *pars facialis*. It might have formed a pterygoid process to articulate with the anterior ramus of the pterygoid, but breakage and the articulation of the lower jaw do not permit us to assess the morphology of

this portion of the maxilla. The anterior half of the bone preserves several fragmentary teeth; the teeth are represented by notably robust elements, wider labiolingually than mesiodistally, with slightly oval cross-sections that diminish in size apically. They appear as low truncated cones, protruding from the maxillary occlusal margin. The teeth are supported and separated from each other by bony ridges and abundant osseous deposits that fill the spaces between the ridges and the tooth bases, surrounding the latter. The tooth tips are not preserved and, thus, the number of cusps is unknown. The even distal ends of some of the best-preserved teeth suggest that these elements might correspond to the pedicels of pedicellate teeth. We were unable to recover any replacement tooth. Posteriorly, the tooth row slightly exceeds the level of the articulation between pterygoid and maxilla. The edentulous posterior half of the maxillary arch extends to near the lower jaw joint, probably including an ossified quadratojugal posterolaterally either in contact or fused to the ossified distal articular portion of the palatoquadrate.

Squamosals. Each of these dermal bones bears an extensively sculptured dorsal plate (*lamella alaris*) that anterolaterally articulates with the maxilla and forms part, or all, of the lateral margin of the orbit (Figs 3A, 4A). This dorsal plate might have extended anteriorly to reach the nasal but the margin of this bone at the anterolateral corner of the orbit is not preserved. The *lamella alaris* arches over the lateral portion of the dorsal surface of the *crista parotica* forming a low angle with it. The medial margin of the *lamella alaris* is slightly concave and anteriorly it might have had a minimal contact with the parietal portion of the frontoparietal if the latter bone extended laterally far enough. Laterally, the *lamella alaris* forms the margin of a round opening entirely delimited by sculptured dermal bone (Figs 3A, 4A). The well-ossified, posterolaterally directed ventral ramus of the squamosal is partially visible through this large opening. A faint shallow groove on the most dorsal portion of the smooth-surfaced ventral ramus probably marks the former site of attachment of the tympanic annulus, but whether some ossification of this cartilaginous ring occurred, as suggested previously (Báez et al. 2005), is difficult to ascertain. The squamosal articulates with the *crista parotica* by means of the ramus paroticus (*sensu* Roček 2003; = otic plate of Lynch 1971, in part); however, this part of the squamosal is not discernible either because it was either poorly developed or was fused to the dorsal surface of the prootic. The ventral ramus of the squamosal has a smooth surface and its distal half increases in width distally; this ramus is fused to the ornamented sheet of bone that forms the rounded posterolateral corner of the skull.

Palatines. The ventral surface of the right postnasal wall is clearly invested by a palatine bone (neopalatine of Trueb (1973)). The latter element has an outline roughly

resembling an isosceles triangle tapering medially, with its base along the maxilla; odontoids are not discernible on its palatal surface, although a short, low ridge extends along the midportion of its posterior margin. The bone is fused neither to the vomer nor to the maxilla. It is evident that the left and right palatines were well separated from each other medially (Fig. 4B).

Vomers. These bones are only represented by a fragment of the lateral part of the right element, not large or intact enough to provide any significant morphological information.

Parasphenoid. This T-shaped bone invests the ventral surface of the endocranium (Figs 3B, 4B). It extends anteriorly by means of a cultriform process; the most anterior portion of this process is slightly broken but the impression left on the ventral surface of the sphenethmoid indicates that its anterior end had a rounded margin and reached almost to the level of the palatines. The width of the cultriform process increases posteriorly, reaching its maximum at its midlength, and then decreasing from this point backwards. No keel or ridge is discernible on the gently convex ventral surface of the process. The subotic alae are anteroposteriorly wide and invest the floor of the otic capsules to which they appear to have been synostotically united. The alae are perpendicular to the longitudinal axis of the cultriform process; no ridges are evident on their ventral surfaces, although the region between each ala and the cultriform process is not well preserved. Anteriorly, each ala has an extensive articulation with the sturdy medial ramus of the corresponding pterygoid (Figs 3B, 4B), whereas posteriorly the ala reaches near to the anterior margin of the condyloid fossa. The presence of a well-developed posteromedial process at the level of the ventral margin of the foramen magnum cannot be assessed owing to the overlapping atlantal vertebra in this area.

Pterygoids. These triradiate bones are notably robust elements of the skull; each possesses well-developed anterior, medial and posterior rami (Figs 3B, 4B). The anterior ramus is wide and anterolaterally articulates broadly with the *pars palatina* of the maxilla, reaching near the palatine; in turn, an anteromedial part of this ramus is directed dorsally to contact the ventral surface of the *pars facialis* of the maxilla. The conspicuous medial ramus rests on the anterior wall of the otic capsule and has an extensive articulation with the anterior edge of the corresponding ala of the parasphenoid. The relatively long posterior ramus invested the palatoquadrate medially; this ramus is fused to the ventral ramus of the squamosal and terminates at the angle of the jaw, which is located posterior to the level of the occiput. At the level of the junction of the anterior ramus with the posterior ramus, the lateral margin of the pterygoid bears a distinct ear-like expansion, or ventral

flange, which extends near to the coronoid process of the angulosplenial when the mouth is closed.

Endocranium

Sphenethmoid. The braincase is relatively narrow and extensively ossified (Fig. 3A, B). Anteriorly, the sphenethmoidal ossification invaded the *tectum nasi* to which the overlying nasals are fused. The bony nasal septum extends between the ossified *tectum nasi* and *solum nasi*, separating the right and left olfactory capsules and reaching the anterior tip of the nasals; also ossified is the part of the *solum nasi* adjacent to the *septum nasi* (*crista intermedia*). The posterior wall of each nasal capsule, pierced by the orbitonasal foramen for the medial branch of the ophtalmicus profundus nerve, is also ossified. Posterior to the nasals, the sphenethmoid roofs the *cavum cranii* completely without being evident the presence of a frontoparietal fenestra in the preserved portion of the braincase, which reaches a level somewhat posterior to the estimated posterior margin of the bony orbit (Fig. 3A). The extent of the ossified roof of the braincase suggests that chondrification of the *tectum cranii* during development, at least at the level of the frontal fenestra, might have obliterated or reduced this opening. The sphenethmoid appears to have been exposed dorsally between the divergent anterior portions of the frontoparietals. In turn, the ventral surface of the sphenethmoid is invested by the cultriform process of the parasphenoid. At the level of the posterior margin of the orbits, shallow indentations at both sides of the edge of the sphenethmoid probably correspond to the anterior margins of the foramina for the optic nerves. Incomplete preservation, however, prevents description of the posterior extent of the sphenethmoid and its relationship with the otic capsules.

Otoccipitals. The prootics and exoccipitals are completely fused to one another to form the otic capsules. The anterior wall of the relatively well-preserved left otic capsule is pierced by the large prootic foramen; an ossified prefacial commisure separating the prootic foramen from the palatine foramen is not present. Lateral to the prootic foramen there is another opening of smaller size enclosed by bone, which might correspond to the passage for the jugular artery. The prootic extends dorsolaterally to form the long, distally expanded, well-ossified *crista parotica*, which remained partially exposed dorsally between the squamosal and frontoparietal (Figs 3A, 4A). Dorsomedially, at the level of the lateral margin of the occipital condyle, there is a prominence for the posterior semicircular duct, which forms a conspicuous, posterolaterally directed crest. Displaced elements of the pectoral girdle obscure the ventrolateral portion of the otic capsule. Lateral to the base of the right occipital condyle there is a

deep condyloid fossa; no perilymphatic opening piercing the posteromedial wall of the otic capsule lateral to the condyle and posterior to the jugular foramen is visible. The number and location of the foramina on the partition between the brain and the labyrinth cavities are unknown owing to the sediment that fills these spaces. The occipital condyles are narrowly separated and not stalked. The foramen magnum appears to have been completed by cartilage mid-dorsally.

Lower jaw

The two mandibular arches, each of which is formed at least by a well-ossified dentary and angulosplenial, form the lower jaw. The dentary extends for about one-half of the length of the jaw; this laminar bone is dorsoventrally high but its poor preservation prevents us from determining whether it had serrations along its sharp dorsal or occlusal edge. The anterior tip of the left dentary, which is better preserved than the right one, is broken; therefore the extent of the mentomeckelian as well as the presence of an odontoid in the symphyseal region cannot be ascertained. The angulosplenial is slightly recurved inwards along most of its length, whereas in the articular process region it is oriented posterolaterally (Fig. 3B). The coronoid process is partially concealed by the pterygoid and the maxillary arch on both sides of the skull but it is evident that it is relatively short and bump-like. An elongated depression ventromedially well defined by a marked ridge, probably the area for the insertion of the masticatory masseter muscle, extends lateral (external) to the coronoid process and reaches the articular region. Photographs taken before preparation of the specimen show the presence of mentomeckelian bones, although it is not possible to determine their extent and relationships accurately. This part of the lower jaw was lost subsequently.

Postcranium

Vertebral column. The vertebral column consists of eight discrete presacral vertebrae, sacrum and urostyle (Figs 2B, C, 4A). These axial components are partially disarticulated and preserved in different orientations (Fig. 5A). The anterior four presacral vertebrae and the sacrum are preserved mainly in ventral or slightly ventrolateral aspect in one of the two pieces of sandstone (DNPM Pal. 1412-R B; Fig. 2B), whereas the rest of the presacrals are exposed in dorsal or posterior views and part of the urostyle is visible in right lateral aspect in the other piece (DNPM Pal. 1412-R A; Fig. 2C). The centrum of Vertebra V is not preserved, whereas those of Vertebra IV and of the last two presacrals (VII, VIII) are mostly incomplete. The centra are robust and slightly depressed dorsoventrally. The first presacral vertebra, the atlas, is articulated with the succeeding vertebra but disarticulated from the skull; however, the closely juxtaposed posterior

part of the skull prevents assessment of the detailed configuration of the articular cotyles (Fig. 5A). Despite this fact, the convex shape of the anteroventral margin of the atlas and lack of an intercotylar notch indicate that a type I cervical vertebra of the scheme by Lynch (1971), which usually has stalked cotyles, is not likely present. The atlantal neural arch, visible in lateral and dorsal views, bears a high, flat-topped neural spine; this spine is triangular in dorsal view with the posterior margin partially fused to the neural spine of the succeeding vertebra. The neural spine of Vertebra II is also high and dorsally directed; its top is flat and rectangular in dorsal view. An anteriorly concave line marks the articulation of the atlantal centrum with the centrum of Vertebra II. Unlike the atlas, all the other presacrals bear transverse processes.

The transverse processes of Vertebrae II, III and IV are remarkably robust and anteroposteriorly wide, although those of Vertebrae III and IV are mediolaterally longer than the transverse processes borne by Vertebrae II; also, the distance between the contralateral distal ends of Vertebrae III and IV are greater than that between the lateral margins of the sacral diapophyses, whereas the distance between the processes of Vertebra II is seemingly shorter (Fig. 5A). In contrast, the transverse processes of the posterior presacrals (V–VIII) are distinctly narrower and the shape of the preserved portions indicates that they were not expanded distally. The right transverse process of Vertebra IV is entirely preserved; its distal end is slightly expanded, tapering posteriorly; this indicates that the elongated and usually cartilaginous distal end of the transverse process is ossified. The right transverse process of the succeeding vertebra (V), also almost entirely preserved, is mediolaterally shorter than the process borne by Vertebra IV and, unlike it, has a rounded cross section; a narrow flange is present along the posterior margin of its proximal half. The transverse processes of the posteriormost three presacral vertebrae are distally broken, but it is evident that they are shorter than those borne by the anterior vertebrae. The lengths of the transverse processes, from highest to lowest are: IV > III > V > II > VI–VII–VIII. With regard to their orientation, the transverse processes of Vertebra II are slightly anteriorly directed, those of the Vertebra III are nearly perpendicular to the longitudinal axis of the vertebral column, and those of Vertebra IV are slightly directed posteriorly. In turn, the transverse processes of Vertebrae V and VI are oriented posterolaterally, and those of Vertebrae VII and VIII, which also bear posterior flanges, are directed forwards. There is no evidence of free ribs or the presence of a dorsal shield.

The neural arch of Vertebra VI is exposed in dorsal view; the neural arch lamina of this vertebra is somewhat wider than long and its width does not diminish markedly between the pre-and post zygapophyses (Fig. 6D). The neural spine is broken off but, judging from the neural spine of the succeeding vertebra (VII), it must have been

thick, dorsally directed, and distally flattened. The pre- and postzygapophyses are well developed and have oval, flat articular surfaces that lie in a slightly inclined plane.

With regard to the articulation between successive centra, it is clear that the anteriorly concave irregular contact between the atlantal centrum and that of Vertebra II suggests the presence of a condyle at the posterior end of the former and a cotyle at the anterior end of the latter (i.e. procoelous condition). The posterior end of the centrum of Vertebra II, however, shows a fine line between the ventral surface of the centrum and that of a short element of a distinctly different texture and colour to which a piece of bone probably belonging to the following vertebra is attached. The centrum of Vertebra III is disarticulated from the preceding vertebra and, therefore, it is possible to ascertain the presence of a concave anterior articular facet whereas an element of different texture appears to be intercalated between the centrum of this vertebra and that of Vertebra IV (Fig. 5A). This evidence suggests that mineralized intervertebral elements might have occurred in earlier developmental stages of this fossil species, as in some extant basal neobatrachians (Muzzopappa *et al.* 2016; AMB pers. obs.). The posterior end of the centrum of Vertebra IV is transversely broken but no notochordal pit is present. The centrum of the last presacral (VIII) is preserved as an external mould; it was buried anteroposteriorly into the sediment and a bony condyle that might correspond to the articulation with the preceding vertebra is discernable at the level of its anterior end.

The sacrum is composed of a single vertebra (IX), which is incompletely preserved (Fig. 2B). The anterior part of the sacral centrum is missing, whereas posteriorly it bears two condyles for the articulation with the urostyle. The sacral diapophyses are proximally robust but their thin distal margins, partially preserved, indicate that they are dorsoventrally flattened. They are moderately expanded distally, more posteriorly than anteriorly, oriented almost perpendicularly to the longitudinal axis of the column and with a slightly concave posterior margin in dorsal view. The length of the distal margin is about 1.75 times that of the proximal portion. The diapophyses are slightly dorsally deflected.

Only the anterior part of the urostyle is preserved (Fig. 2C) and, thus, the general proportions of this element could not be determined although the elongate length of the iliac shafts suggests that it was not particularly short. The preserved portion lacks transverse processes and bears a dorsal crest, the height of which is greater than that of the shaft at the anterior end; taking into account its great height, the crest probably extended nearly all along the bone length. Anteriorly, a robust anterodorsal process projects from the crest.

Pectoral girdle. Components of the right half of the pectoral girdle exposed in dorsal view are preserved in DNPM Pal. 1412-R A (Figs 2C, 5B, 6A), whereas some of the left half, partially overlapped by skull and forelimb bones, are preserved in DNPM Pal. 1412-R B (Fig. 2B). The scapula has an expanded bicapitate medial (ventral) end, with a deep U-shaped notch separating the *pars acromialis* from the *pars glenoidalis*; this notch is closed ventrally by bone due to the ossification of the procoracoid cartilage (Fig. 5B). The *pars acromialis* is larger than the *pars glenoidalis*. The scapular shaft is narrow next to the *partes acromialis* and *glenoidalis*, whereas distally it expands and strongly curves dorsally. The total dorsoventral length of the shaft is difficult to estimate accurately because the right scapula, which is better exposed than the left, is distally broken. Our restoration takes into account the shape of the dorsal end of the left bone and indicates that it is moderately elongate (Fig. 6A). Distal to the *pars acromialis* the shaft bears a short, thick, anteroventrally deflected crest on its leading edge (Fig. 5B).

Next to the most dorsal portion of the left scapula, there is a well-ossified, large cleithrum that must have invested part of the anterior edge and dorsal surface of the suprascapular cartilage (Figs 2A, 6A). However, the cleithrum appears not to have overlapped a small anterolateral region of this cartilage, close to the dorsal margin of the scapula, although the extent of the area of the anterolateral margin of the suprascapula invested by the cleithrum cannot be assessed in detail owing to the superimposed skull; in addition, the distinctly convex proximal margin of the cleithrum suggests that it might not have contacted the scapula. The distal margin of the cleithrum is slightly concave, defining a long, dorsally domed anterior portion and a narrow posterior plate (Fig. 6A).

The clavicle is markedly robust and strongly bowed anteriorly. Its dorsal end must have extended over the ossified procoracoid cartilage; this end of the clavicle is fused to the *pars acromialis* of the scapula. The ventral (medial) tip of the curved shaft of the clavicle reaches farther anteriorly than the level of the anterior margin of the scapula. Only the incomplete right coracoid is preserved represented by its stout glenoidal end; its sternal end is missing. Neither prezonal nor postzonal elements of the pectoral girdle are preserved.

Forelimbs. Humeri and radio-ulnae are the only preserved components of the forelimbs. The incomplete left humerus is exposed in ventromedial aspect on DNPM Pal. 1412-R B. The humeral head (= *caput humeri*) has a distinct dorsal curvature with respect to the longitudinal axis of the diaphysis (Fig. 6C); its articular surface extends ventrally and reaches the proximal end of the relatively well-developed deltoid crest (= *crista ventralis* or deltopectoral crest). The latter crest extends along the proximal one-third of the diaphysis length, gradually diminishing in height distally. A proximodistally shorter accessory crest (= parietal crest) flanks the deltoid crest medially,

forming a well-defined, short groove; this groove probably housed the long tendon of the coraco-radialis muscle. The ventral edge of this accessory crest is wide and flat. The distal portion of the left humerus is not well preserved and the degree of expansion of the medial epicondyle is unknown. The right humerus is exposed in lateral view on DNPM Pal. 1412-R A (Fig. 5B). It is a robust bone, the head of which is almost completely covered by sediment. The edge of the laterally deflected deltoid crest is notably thick, particularly at the level of the proximal end of the accessory crest, suggesting a great development of the deltoid and pectoralis musculature that inserts there. A distinct oval concave area, which might correspond to the site of insertion of the clavicularis slip of the deltoid muscle (Sigurdsen et al. 2012), occurs lateral to the deltoid crest. On the ventral side of the distal end of the bone, a hemispherical condyle (*eminentia capitata*) is partially obscured by the radial part of the articulated radioulna; the condyle is relatively large and completely ossified, whereas it is evident that a long cubital fossa was not present. The lateral epicondyle appears moderately expanded and almost reaches the level of the distal margin of the ventral condyle. A fine ridge extends along the lateral margin of the distal portion of the diaphysis and the ectepicondyle. The radio-ulna bears an ossified olecranon process on its proximal end, whereas the shaft becomes gradually expanded distally. A shallow sulcus extends along the distal half of this bone revealing its compound origin. The poor preservation of the distal ends of both radioulnae prevents description of the articular facets for the proximal carpals.

Pelvic girdle. The pelvis is almost entirely preserved and exposed in ventral and right lateral views (Figs 2B, 7A, B). This structure is robust and each half is formed mainly by the ilium and ischium, which collectively contribute to the rounded, shallow acetabulum. In acetabular view, the ilium has a narrow preacetabular zone (*sensu* Lynch 1971), but the ventral acetabular expansion was seemingly broad judging from the sharply increasing width of the preserved portion. The anterior margin of this portion and the iliac shaft form an angle of nearly 70°. The dorsal acetabular expansion of the ilium is oriented posterodorsally, having a modest development and lacking a marked dorsal vector (*sensu* Lynch 1971). A distinct suture between the ilium and the ischium is not discernable, indicating that these bones are probably fused to one another; this obscures their respective boundaries. The acetabular fossa is well delimited ventrally by a prominent rim, but the rim is scarcely evident at its anterodorsal margin. The ilium has a moderately long shaft, which is curved proximally but almost straight along most of its length. Along the dorsal margin of the proximal five-sixths of the length of the iliac shaft there is a well-developed crest whose height gradually decreases distally; this

crest reaches its greatest height at its middle length, where it is about as high as the shaft (Fig. 7A, B). A distinct dorsal prominence that merges anteriorly with the dorsal crest and bears a well-defined dorsal protuberance lies anterior and dorsal to the acetabulum. The dorsal protuberance is elongate, obliquely oriented and strongly projecting laterally; the proximal tip of the protuberance coincides with the anterior margin of the acetabular fossa. The ischium is well ossified and contributes to the posteroventral sector of the acetabulum, although the margin of the latter is broken off. This bone bears a large posterodorsal expansion roughly quadrangular in shape but part of its posterior-most region is missing. The pubic region is poorly preserved; the ossified conserved portions are restricted to the ventral acetabular rim. Based on the morphology and extension of ilia and ischia, the pubic region (cartilaginous or mineralized) might have contributed significantly to the anteroventral sector of the acetabulum.

Hind limbs. These skeletal parts are incompletely preserved; thus, we were unable to estimate their proportions with respect to body size. Both femora are preserved although the right is more complete than the left. Each femur has a slightly sigmoid shape and bears a short, but distinct, ventral crest along the proximal third of its length (Fig. 4A). The proximal (acetabular), as well as the distal epiphyses are well ossified. The left tibiofibula is nearly complete; it is slightly longer than the femur (38.5 mm and 38.1 mm respectively). A few disarticulated unidentified metatarsals and phalanges of the left hind limb are present.

Remarks

Although our re-examination of the holotype of *Baurubatrachus* confirmed most features described by Báez & Perí (1989), a few points, apart from the new anatomical aspects revealed by the recent preparation of the specimen, merit some comments. The most important of these points, in addition to those discussed below, concerns the participation of the maxilla in the formation of the lateral margin of the orbit. It is clear that the posterolateral margin of the right orbit is formed by an ornamented dermal bone with a slightly concave dorsal margin; this bone might be either part of the *pars facialis* of the maxilla, as it was interpreted originally (Báez & Perí 1989), or part of the anteriorly extended *lamella alaris* of the squamosal, as suggested subsequently (Báez et al. 2005). The extensive ornamented bone that is well preserved on the left side of the skull arching over the dorsal surface of the prootic, but missing on the right side, is part of the squamosal (*lamella alaris*); contact between this part of the squamosal and the sheet of bone that forms the orbital margin is not discernible. However, on both sides of the skull a similar crack might coincide with an extensive contact between the maxillary *pars facialis* and the

squamosal, suggesting an anterior extension of the latter bone and the restriction of the contribution of the maxilla to the orbital margin. The available evidence precludes a conclusive statement regarding this feature.

Comparative morphology

It is evident that many striking features of *Baurubatrachus* might be related to skeletal hyperossification, i.e. bone growth or some other form of calcification, which may involve cartilage, in excess to that found in the ancestor. Conditions such as the heavily sculptured cranial elements, the broad contact between nasal and maxilla and between the latter with the squamosal, the extensive *lamella alaris* of the squamosal, the well-developed supraorbital flange of the frontoparietal, the ossified roof of the *cavum cranii*, and the reduction, or absence, of the subtemporal fenestra collectively can be interpreted as manifestations of this phenomenon, which may occur within lineages in different parts of the anuran tree (Báez & Perí 1989). The implications for the investigation of the phylogenetic relationships of *Baurubatrachus* are twofold: not only have many of these conditions appeared repeatedly in anuran lineages not closely related according to recent molecular analyses but also they might be part of a suite of correlated characters. In morphological parsimony analyses many of these traits have been recovered as strong support for clades not corroborated by molecular data, although this might be a result of developmental correlation through heterochronic changes (Smith *et al.* 2007).

One of the most peculiar features of *Baurubatrachus* is the configuration of the otic region of the skull, with the tympanic membrane probably completely circumscribed by bone in life (Fig. 4A). This condition seldom occurs amongst anurans. In the aquatic pipids the squamosal ossification invades the tympanic annulus to form a funnel-shaped compound tympano-squamosal bone (Cannatella & Trueb 1988) that incompletely encircles a dense tympanic membrane. In the fossorial endemic Cuban bufonid toad *Peltophryne empusa* the extensively ornamented *lamella alaris* of the squamosals completely surround the margins of round openings to which the tympanic annuli and tympanic membranes are attached on both sides of the skull. In this species a well-developed otic plate contacts the *crista parotica*, whereas anterior and posterior portions of the *lamella alaris* extend ventrally to contact one another after enclosing the tympanic opening; the posterior extension of the *lamella alaris* is partially fused to the ventral ramus of the squamosal (AMB pers. obs.). In other species of *Peltophryne*, however, the squamosal does not enclose the tympanic ring completely (Pregill 1981; Pramuk 2002). Fusion of a lateroventral extension of the *lamella alaris* and the ventral ramus of the squamosal also occurs in other neobatrachian taxa, such as the hemiphractid *Hemiphractus johnsoni* (AMB pers. obs.).

Another noteworthy feature of the skull of *Baurubatrachus* is the extreme reduction or absence of the subtemporal fenestra. This feature occurs in phylogenetically distant neobatrachian lineages to a variable degree and may be variable even among species of a single genus. For example, it is present in some bufonids (Pregill 1981; AMB pers. obs.), ceratobatrachids (Laurent 1943; AMB pers. obs.), craugastorids (Lynch 1975), hemiphractids (Trueb 1974; Sheil & Mendelson 2001), microhylids (Zweifel 1971; AMB pers. obs.), although the degree of reduction of this fenestra and the configuration of this region varies, showing the plasticity of the dermal elements involved. Among the ceratophryid taxa, *Lepidobatrachus asper* has a reduced subtemporal fenestra (FCEN 630); in this species the *pars facialis* of the maxilla extends more posteriorly than in other members of this clade and, consequently, this opening is relatively shorter anteroposteriorly. A relatively small fenestra occurs also in *L. llanensis* (FCEN 1293).

The absence of a discernible perilymphatic opening in the posteromedial wall of the otic capsule anterolateral to the occipital condyle is another feature that merits attention. In most frogs either the large inferior perilymphatic foramen (e.g. *Alytes*, *Discoglossus*, pelobatids, australobatrachians) or two closely spaced foramina corresponding to both inferior and superior perilymphatic foramina (e.g. ceratophryids, bufonids) open into an extracranial space posterior to the jugular foramen. This suggests a different route for the perilymphatic canal in *Baurubatrachus*.

The extensive ossification of the dorsal wall of the braincase suggests that during the ontogeny the roof of the *cavum cranii* became almost completely chondrified, although it is not possible to assess the contribution of the various cartilaginous structures. No frontal fenestra on the roof of the braincase is evident in the only known specimen of *Baurubatrachus*. The same condition has been described in a few anuran taxa, in which is reached by at least the metamorphic climax (Haas 2003), such as the ceratophryids *Ceratophrys cranwelli* (Wild 1997; Fabrezi & Quinzio 2008), *C. cornuta* (Wild 1997), *Lepidobatrachus llanensis* (Fabrezi & Quinzio 2008), *L. laevis*, *Chacophrys pierottii* (Fabrezi & Quinzio 2008), and the australobatrachian *Calyptocephalella gayi* (Reinbach 1939).

The maxillary dentition in *Baurubatrachus* is only represented by several poorly preserved teeth that lack their apical portions. The articulated lower jaw prevents evaluation of the relative height of the *pars dentalis*. It is noteworthy that the adult dentition of all extant species of ceratophryids that we examined is characterized by conical teeth, usually lingually recurved in *Ceratophrys* and *Lepidobatrachus*, attached to a distinctly relatively shallow *pars dentalis*; in these species the teeth are monocuspid and lack a macroscopically obvious separation between a basal pedicel and apical crown (Fig. 8A–D) unlike in the more widespread pedicellate condition (Fig. 8E, F). Because the *pars dentalis*
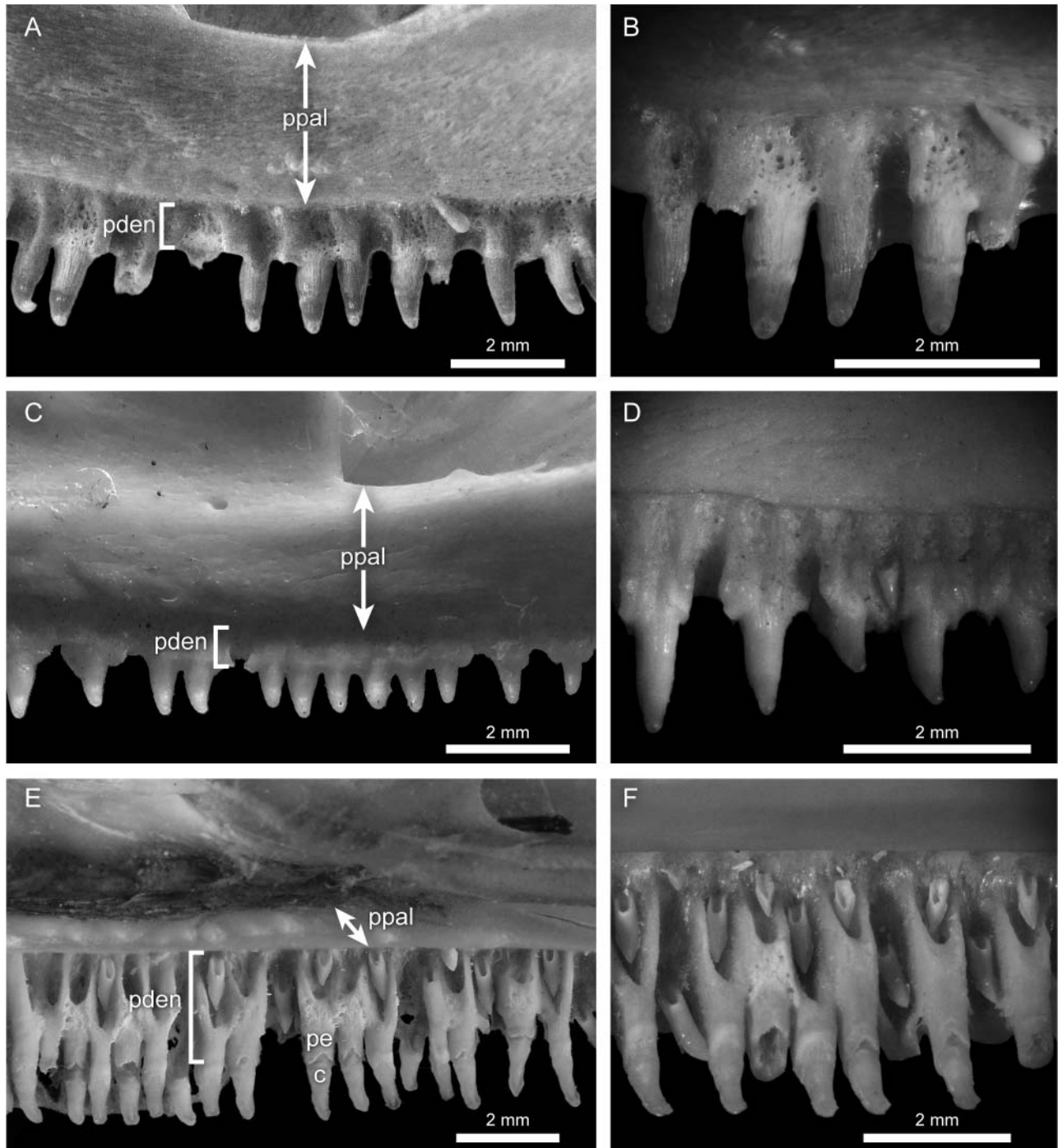
Figure 8. Lingual views of maxillary dentition in the orbital region of selected extant anuran taxa. **A,** *Lepidobatrachus laevis*, FCEN 1442, showing the shallow *pars dentalis* and dorsally directed *pars palatina*; **B,** close-up of same specimen as A showing the bone surrounding the tooth bases and conical shape of replacement tooth; **C,** *Ceratophrys ornata*, FCEN unnumbered specimen, general aspect showing the shallow *pars dentalis* and dorsally directed *pars palatina*; **D,** *Ceratophrys* sp., FCEN unnumbered specimen, close-up showing the bone surrounding the tooth bases, the shallow *pars dentalis*, and the flattened *pars palatina*; **E,** *Calyptocephalella gayi*, MACN 45746, general aspect showing the lack of bone on the lingual side of the tooth bases, pedicellate condition, and deep *pars dentalis*; **F,** *Calyptocephalella gayi*, MACN 45746, close-up showing the hollow tooth pedicels and replacement teeth. Abbreviations: c, tooth crown; pe, tooth pedicel; pden, *pars dentalis*; ppal, *pars palatina*.

is very shallow, only a relatively shallow portion of the basal part of fully erupted teeth is supported by bone; this support includes not only the ridges borne by the *pars dentalis* but also attachment bone surrounding each tooth (Fig. 8A–D). This configuration differs from that of the Cretaceous *Beelzebufo*, whose dentition was considered *Ceratophrys*-like by Evans *et al.* (2014), in which the deep *pars dentalis* supports the very narrow mesiodistally tooth bases (Evans *et al.* 2014, fig. 31). In *Baurubatrachus*, as in *Beelzebufo*, the tooth tips are not preserved but the remaining bases have even apical margins and cross sections lacking an evident ample hollow pulp cavity. According to our examination of skulls of different living ceratophryid taxa, the cancellous mineralization filling the pulp cavity and the firm attachment prevent the teeth from falling or breaking off easily, unlike the preserved condition in these Cretaceous taxa.

The pectoral girdle of *Baurubatrachus* also has distinctive features. The disposition and general shape of the bony components indicate that an arciferal type of girdle was present as in many groups of frogs. However, the peculiar morphology of the scapula, specifically its marked dorsoventrally curved shaft and ventrally deflected hypertrophied crest along the proximal one-half of its leading edge (Fig. 5B), sets it apart from most comparative material available to us. Unlike the lamina that extends along almost the entire leading margin of the scapula of some anurans, lying in the scapular main plane (e.g. *Calyptocephalella gayi*), the crest borne by the scapula in *Baurubatrachus* occurs next to the *pars acromialis*, has a convex edge and is strongly deflected ventrally to form a deep depression on the anterior margin of the scapula that might have increased the site for muscle attachment. This feature of the scapula resembles an analogous, but less developed, expansion that we have observed in *Telmatobius verrucosus* and has been noted in some other species of this genus ("leading (i.e. anterior) edge of the scapula [...] hypertrophied") by De la Riva *et al.* (2012, p. 104). It is noteworthy that in species of *Telmatobius*, particularly in males, laminar crests for muscle attachment occur on the humerus but no such crests occur in the only known specimen of *Baurubatrachus*. Also in large individuals of the hyperossified australobatrachian *Calyptocephalella gayi* the anterior crest of the scapula, which in this taxon extends nearly along the entire shaft, is slightly, but distinctively, inclined ventrally, thus defining a semicircular, shallow depressed area on the dorsal surface of the bone.

The deep basin formed by the anterior crest of the scapula in *Baurubatrachus* might be associated with the enlargement of the muscles that attach to this part of the bone. One such muscle is the *sternocleidomastoideus*, which arises from the squamosal and tympanic ring and inserts into the anterior border of the scapula (Ecker 1889), as well as the *cucullaris*, which usually inserts on the anterodorsal surface of the scapula (Emerson 1976); both muscles are flexors of the head. Also, the *scapularis*

portion of the deltoid muscle, the action of which is to draw the limb forwards, arises chiefly from the dorsal surface of the scapula and lastly on its anterior border to insert into the deltoid crest of the humerus (Ecker 1889), which is well developed in this specimen. The general habitus and capacity for flexing the head might be related to some protective behaviour, perhaps within burrows, using the head to close the holes to avoid desiccation during seasonal drought. Interestingly, this behaviour was observed by Barbour (1914, 1926) in the toad *Peltophryne empusa*, which inhabits a tropical semi-arid environment and shelters in holes in the ground, although in this taxon the skull is proportionally high as in many bufonids unlike that of *Baurubatrachus*. Few other anurans, mostly tropical hylids, have been reported to have this behaviour, which is called phragmosis (Jared *et al.* 1999).

The possible transient presence of independent intervertebral cartilages that might be mineralized during development in *Baurubatrachus* is a meaningful feature. These cartilages may have tended to attach into the anterior end cavity of each centrum, becoming firmly associated with the bony centrum in front with increasing age, as it seemingly has happened with the element between Vertebrae I and II, resulting in the procoelous condition of the latter. Free intervertebral discs in post metamorphic individuals that may ankylose to adjacent centra occur in most extant anomocoelans, such as *Pelobates cultripes* (Rodriguez Talavera 1990), *Spea bombifrons* (Wiens 1989), *Scaphiopus couchii* (Rodriguez Talavera 1990) and *Megophrys major* (Griffiths 1959). However, free intervertebral discs have not been described in the formation of the procoelous centra of the anomocoelan *Pelodytes punctatus* (Rodriguez Talavera 1990), although have been considered present by Lynch (1973). These elements also occur in the development of the axial skeleton in some neobatrachians, such as australobatrachians; e.g. all of the myobatrachines and many of the limnodynastines of Lynch (1971).

The disarticulated axial skeleton and the lack of preservation of the distal segments of the limbs prevent knowledge of their relative proportions, although it is evident that the tibiofibula is not markedly shorter than the femur in *Baurubatrachus* as it is in many good diggers or walkers (Emerson 1976), such as some ceratophryids. Also, the relative proportions of femur and ilium are similar to those of most non-jumper anurans.

Phylogenetic analyses

Previous results on the phylogenetic placement of *Baurubatrachus*

Originally Báez & Perí (1989) discussed *Baurubatrachus* in relation to Ceratophryidae and other hyperossified 'leptodactylids' (*sensu* Lynch 1971), but suggested that

the presence of noticeably expanded transverse processes on the anterior presacral vertebrae might indicate relationship to the former group. At that time this feature was considered a possible synapomorphy of the ceratophryid clade (Lynch 1982; Wild 1999), although it had not been retrieved in a phylogenetic analysis. However, Báez & Perí (1989) recognized that *Baurubatrachus*, even if its relationship with ceratophryids could be demonstrated, was not a member of the crown-group because derived features of the ceratophryid clade such as the non-pedicellate dentition or the lack of a lingually directed palatine shelf of the maxilla are not evident in the only known specimen.

A few decades later, Evans *et al.* (2008), in their original description of *Beelzebufo ampinga* based on disarticulated remains collected in several localities of the Maastrichtian Maevarano Formation of Madagascar, presented a morphology-only maximum parsimony analysis in which *Baurubatrachus* was part of the taxonomic sample. This analysis was based on the matrix by Fabrezi (2006), which included 40 species of extant genera scored for 81 mostly osteological characters, with the addition of 21 extant genera and four fossil taxa, among them *Baurubatrachus*. The analysis of Evans *et al.* (2008) resulted in 106 most-parsimonious trees, retrieving *Baurubatrachus* as a member of crown-group Ceratophryidae, although this clade was included in a more inclusive clade that only has hyperossified, distantly related hyloid neobatrachians as members. Subsequently, considering the importance of the taxonomic placement of fossils used for calibrations of molecular phylogenies, Ruane *et al.* (2011) reanalysed the dataset presented by Evans *et al.* (2008) using maximum parsimony as well as Bayesian inference methods. In their analyses based on morphology, *Baurubatrachus* was allied with ceratophryids. In contrast, the analysis of a combined dataset of morphological and molecular characters including only those extant taxa for which this information was available plus four extinct taxa resulted in the placement of *Baurubatrachus* on the stem that supports extant ceratophryids (Ruane *et al.* 2011). More recently, Laloy *et al.* (2013) described CT scanned new material assigned to the Eocene *Thaumastosaurus gezei* from France, the taxonomic placement of which was still elusive. These authors presented a morphology-only analysis based on a previous matrix by Báez *et al.* (2009), including a higher number of extant and extinct taxa, but with genera, instead of species, used as terminals. In that study *Baurubatrachus* was recovered as a member of crown Ceratophryidae, allied to *Chacophrys*, within a clade of hyperossified taxa whose placements differed significantly from those in recent broad-scale molecular phylogenies (e.g. Frost *et al.* 2006; Pyron & Wiens 2011).

The monophyly of Ceratophryidae and the inclusion of *Baurubatrachus* within this clade were also recovered by Evans *et al.* (2014) in their study of additional material assigned to the putative ceratophryid *Beelzebufo*. These authors conducted phylogenetic analyses based on morphology and genetic data from nine nuclear and three mitochondrial genes. For the morphology-only analyses they used the dataset of Báez *et al.* (2009) with an expanded taxon sampling (43 additional taxa) to include a higher number of heavily ossified taxa, among them *Baurubatrachus* and the extant *Calyptocephalella*. Maximum parsimony analysis of the morphology-only dataset and maximum parsimony and Bayesian inference analyses of the combined dataset recovered *Baurubatrachus* within Ceratophryidae, as the sister taxon of the living *Chacophrys*.

Agnolin (2012) in his description and comments on new fossil materials from Patagonia depicts *Baurubatrachus* as nested within crown-group Ceratophryidae. We are not considering his conclusions regarding the taxonomic position of *Baurubatrachus* because of the high number of anatomical, as well as methodological, inaccuracies in that work. For example, the terminology used to describe the character states of the palatine shelf of the premaxilla and maxilla is not clear and is not the one used in the literature source cited as support (Lynch 1971) by this author. Also, the putatively "extremely shortened" urostyle of the new *Calyptocephalella* species (Agnolin 2012, p. 143) is not supported by the available evidence; moreover, if present, this condition does not contrast with that of ceratophryids as erroneously suggested by Agnolin (2012) citing Reig (1960). It is not clear whether the single partial cladogram depicted in his paper is one of the trees resulted from his analysis or a consensus; also, no measures of support are given. The taxonomic actions proposed by this author (e.g. referral of a new species to the genus *Calyptocephalella* and the resurrection of *Gigantobatrachus*) are not supported by the only tree shown in the paper (Agnolin 2012, fig. 3). For example, in this tree '*C. satan*' is not a member of the *Calyptocephalella* clade, but the sister taxon of *Beelzebufo ampinga*. As a result, his genus *Calyptocephalella* is paraphyletic. However, contradictorily, in the text Agnolin comments on the sister-group relationship of *Beelzebufo* and his crown-group Calyptocephalellidae (Agnolin 2012, p. 150). From the above, we consider that a critical re-examination of the work of Agnolin (2012) is needed in order to discuss his conclusions, but this is beyond the scope of the present paper.

Results

Unconstrained analyses of full matrix. Our maximum parsimony analysis of the complete dataset, with all characters treated as unordered and equally weighted, yielded six most parsimonious trees (MPT), each 1116 steps long (CI = 0.210; RI = 0.556). The strict consensus of the six

MPTs shows a fairly good degree of resolution but contains groupings that are not supported by molecular data according to recent hypotheses (Fig. 9). In this tree, Costata was recovered as the sister group of a trichotomy that includes Anomocoela, the basal neobatrachian *Hadromophryne* (= *Heleophryne*) *natalensis*, and a large clade containing the remaining neobatrachian taxa included in the analysis. Within the latter neobatrachian clade, *Baurubatrachus* occurs as the sister taxon of the living South American helmeted australobatrachian *Calyptocephalella*; these taxa, in turn, form a more inclusive clade with the Early Cretaceous *Eurycephalella*. Although it is evident that this three-taxon clade is sister to a large clade of hyperossified hyloid and ranoid neobatrachians that have disparate positions in the anuran trees based either on molecular or morphological data (e.g. Frost *et al.* 2006; Báez *et al.* 2009; Pyron & Wiens 2011), *Baurubatrachus* is not allied with the otherwise well-supported monophyletic Ceratophryidae. The ceratophryid clade is supported by 15 synapomorphies that refer to cranial (characters 9, 11, 13, 36, 44, 45, 54, 59), hyobranchial (characters 65, 72), and postcranial (characters 76, 83, 115, 124, 125) structures. None of these transformations is retrieved as support for the relationship of *Baurubatrachus* with *Calyptocephalella*, which is weakly supported by transformations of postcranial characters (characters 112 and 136), or for the latter two taxa and *Eurycephalella* (character 110).

Only when the morphological data are subjected to implied weighting with very low values of the concavity constant (k = 1–2) is *Baurubatrachus* retrieved within Ceratophryidae and as the sister taxon of *Chacophrys* or as the sister taxon of Ceratophryidae (k = 3–4). However, both arrangements are based mostly on ceratophryid synapomorphies that cannot be scored in the only available specimen of *Baurubatrachus pricei*. In contrast, with higher values of the constant (5–7, 19–30), *Baurubatrachus* appears as the sister taxon of *Calyptocephalella*. With k = 7, *Baurubatrachus* is placed within a clade formed by most extant australobatrachians included in the analysis, again in close association with *Calyptocephalella*. The sister-taxon relationship with the latter genus is supported by the same two postcranial transformations as in the analysis considering all characters equally weighted (character 112, 2>1; character 136, 0>1), plus three additional state changes based on cranial features (character 1, 10, 61) are added to support the node including *Eurycephalella*. In turn, the australobatrachian clade has a sister-group relationship with an artificial clade of hyperossified taxa that includes most of the taxa that appear in the clade of hyperossified taxa retrieved by the analysis of the full matrix with equally weighted characters, including a monophyletic Ceratophryidae (Fig. 10).

Unconstrained analyses of character partitions. Because the liability and homoplasy conveyed by different skeletal parts might differ, we performed analyses based on different partitions of the dataset, e.g. excluding characters of different structural units or those that might be affected by dermal hyperossification. Twelve cranial characters (characters 3, 5–11, 49, 50, 54, 55) probably prone to be influenced by hyperossification were removed to test the effect of these characters on the position of *Baurubatrachus*. The parsimony analysis with characters unordered and equally weighted resulted in a higher number of MPTs (2326, each with a length of 986 steps) than those obtained with the complete dataset. The strict consensus of these MPTs retrieves a trichotomy formed by Costata, Anomocoela, and a poorly resolved Neobatrachia. *Baurubatrachus* occurs in a large neobatrachian polytomy that excludes *Heleophryne* (= *Hadromophryne*) *natalensis* but outside the monophyletic Ceratophryidae, which is part of this polytomy (Supplemental Fig. S15). Interestingly, all the well-ossified ranoid species, including *Thaumastosaurus*, and their less ossified relatives, with the exclusion of microhylids, are clustered together in a clade, unlike their disparate placements that result from the analyses of the complete dataset, pointing out the importance of postcranial features to resolve their interrelationships.

Implied weighting under the same conditions, and with a value of the concavity constant of 7, results in the additional clustering of some closely related taxa, such as the well-ossified *Litoria australis* and the more delicate *L. longipes*, whereas *Baurubatrachus* appears in a clade with *Calyptocephalella* and *Eurycephalella*, but not in the ceratophyid clade (Supplemental Fig. S16). The relative basal position of *Beelzebufo* within the neobatrachian clade suggests that its placement close to the ceratophryid taxa might be driven by the presence of cranial characters linked to hyperossification combined with the scarce information on its postcranial anatomy.

The parsimony-based analysis considering only equally weighted, unordered 73 cranial and hyobranchial characters (i.e. excluding all postcranial and the pupil shape characters) produced 33 MPTs, each of 547 steps. The strict consensus of these MPTs (Supplemental Fig. S17) does not recover Anomocoela or Neobatrachia; it shows a large clade of hyperossified taxa including a distal polytomy, of which *Baurubatrachus*, *Calyptocephalella*, *Eurycephalella*, *Beelzebufo*, *Chacophrys* and separate species of *Ceratophrys* are some of its terminals, suggesting that convergent cranial features, many probably related to dermal hyperossification and increased gape size, conceal the phylogenetic signal of other characters. Analysis of this partition with implied weights under the concavity constant k = 7 results in the placement of *Baurubatrachus* within Ceratophryidae, the latter as part of an artificial clade of hyperossified taxa that includes pelobatoids (Supplemental Fig. S18).
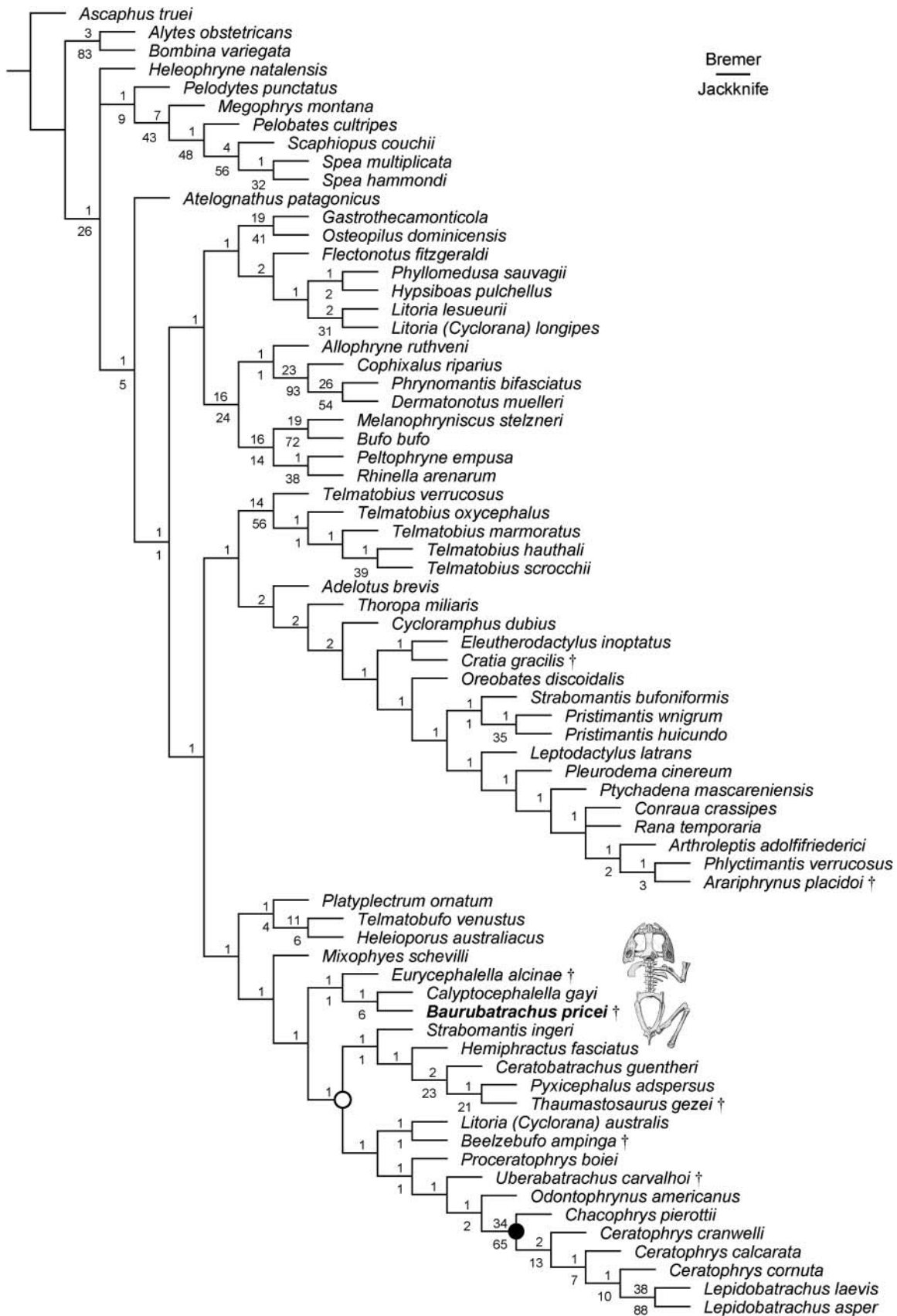
Figure 9. Consensus tree of six MPTs retrieved in the maximum parsimony analysis of the full matrix and all characters considered unordered and of equal weight. Solid circle indicates crown-group Ceratophryidae. Open circle indicates clade of hyperossified taxa.
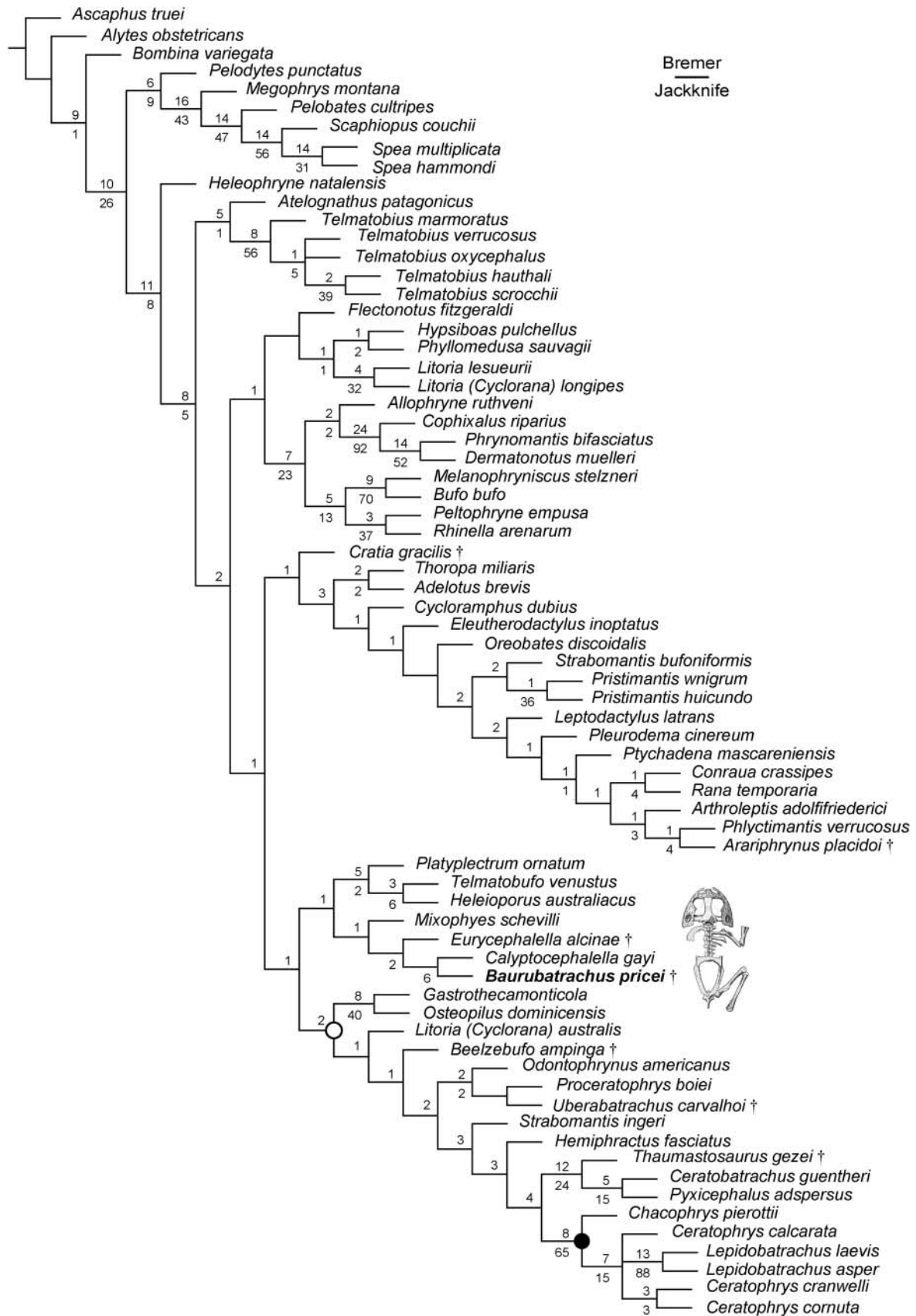
Figure 10. Tree retrieved in the parsimony analysis of the full matrix characters subjected to implied weighting, with concavity constant k = 7. Solid circle indicates crown-group Ceratophryidae. Open circle indicates clade of hyperossified taxa.

When only the 69 postcranial characters, equally weighted and unordered, are considered, the strict consensus of 3930 MPTs of 470 steps shows Neobatrachia with a large distal polytomy including well-ossified as well as poorly ossified hyloid and ranoid taxa. *Baurubatrachus* and *Calyptocephalella*, as sister taxa, are members of this polytomy, as is the clade comprising the ceratophryid living species (Supplemental Fig. S19). Characters subjected to implied weighting with the concavity constant = 7 results in 10 MPTs, in the consensus of which Neobatrachia is retrieved with *Heleophryne* as the most basal taxon followed by a paraphyletic sequence of australobatrachians including (*Baurubatrachus* + *Calyptocephalella*) and (*Beelzebufo* + *Telmatobufo*) (Supplemental Fig. S20).

These analyses of different subsets of characters pertaining to different skeletal units suggest that both cranial and postcranial characters convey phylogenetic information that contributes to retrieve the grouping of closely related species according to molecular evidence, and to resolve the position of *Baurubatrachus*.

Constrained analyses. In order to test previous results, we also conducted a search with the full matrix and equally weighted, unordered multistate characters but forcing the placement of *Baurubatrachus* within Ceratophryidae. This search produced a strict consensus of 72 MPTs, five steps longer than the MPTs retrieved by the unconstrained analysis of the full matrix (Supplemental Fig. S21).

Optimization of the full number of characters over a constrained topology based on the molecular anuran phylogeny of Pyron & Wiens (2011) and that of Faivovich *et al.* (2014) for the interrelationships of the living ceratophryid taxa, considering characters equally weighted and unordered, resulted in one MPT 1259 steps long in which *Baurubatrachus* is the sister taxon of *Calyptocephalella* within clade of calyptocephalellid australobatrachians. It is noteworthy that in this topology, *Beelzebufo* appears as the sister taxon of Ceratophryidae (Fig. 11). Implied weighting using the constant k = 7 also supports the placement of *Baurubatrachus* and *Eurycephalella* within the clade of calyptocephalellid australobatrachians, whereas *Uberabatrachus* and *Beelzebufo* also occur within the australobatrachian clade, although nested within the myobatrachoid subclade (Fig. 12); this is an interesting arrangement as it clusters several Cretaceous taxa from Gondwanan-derived continents.

Synthesis of results. All unconstrained analyses with equally weighted and unordered characters, either with the full matrix or excluding all cranial characters or only those possibly linked to hyperossification, resulted in a monophyletic Ceratophryidae, although the degree of resolution and the topology of the trees varied. In these trees, *Baurubatrachus* is not retrieved as a member of the ceratophryid clade. Instead, it is recovered as the sister taxon

of the australobatrachian *Calyptocephalella*, except when the cranial hyperossification-linked characters are removed from the matrix. In the latter case the position of *Baurubatrachus* remains unresolved as well as that of many neobatrachians, well ossified or not, included in the analysis, but it does not join the ceratophryid clade. It is significant that the relationship with calyptocephalellids also is recovered as a result of the analysis with maximum parsimony searches constrained by using the anuran phylogeny retrieved by Pyron & Wiens (2011) combined with the interrelationships of ceratophryids recovered by Faivovich *et al.* (2014) as a molecular scaffold.

In unconstrained analyses of the full matrix, either with equally weighted characters or characters subjected to implied weighting (k = 7), as well as those constrained under the same conditions, we recovered five autapomorphies for *Baurubatrachus* (marked with an asterisk in the diagnosis above): pterygoid anterior ramus bearing a ventral flange (15:1), at least half of *planum anteorbitale* mineralized (33:1), ossified *septum nasi* (34:2), acute angle between iliac shaft and ventral acetabular expansion (124:0), dorsal prominence scarcely visible from iliac outline and elongate protuberance laterally projected (129:4). An additional two autapomorphies are retrieved only in the unconstrained analysis under implied weights (k = 7) and constrained analyses (equal weights and implied weights, k = 7): maxilla with high *pars facialis* along most of its length and concave posterior margin of ischium (49:3). The peculiar morphology of the scapula (114:4) also is recovered as autapomorphic in the latter analysis.

Discussion

### Is *Baurubatrachus* a ceratophryid frog as previously proposed?

We retrieved 15 synapomorphies for the ceratophryid node from the unconstrained analysis of the full matrix (9:2; 11:1; 13:0; 36:4; 44:1; 45:1; 54: 1; 59:1; 65:1; 72:1; 76:0; 83:1; 115:3; 124:2; 125:2). When the characters are subjected to character weighting (k = 7), Ceratophryidae is also supported by 15 synapomorphies but only six unambiguous derived conditions are common to both analyses: premaxillary *pars palatina* partially fused to the alary process (45:1), ectopic symphyseal ossifications (59:1), alary processes of hyoid absent (65:1), calcifications on hyoid plate (72:1), long transverse process on presacral IV (83:1), and well-developed ventral acetabular expansion of the ilium (124:2); however, most of these character states cannot be determined in *Baurubatrachus*, except for the last two.

When the analysis is constrained by the molecular scaffold under equal weights, Ceratophryidae is supported by
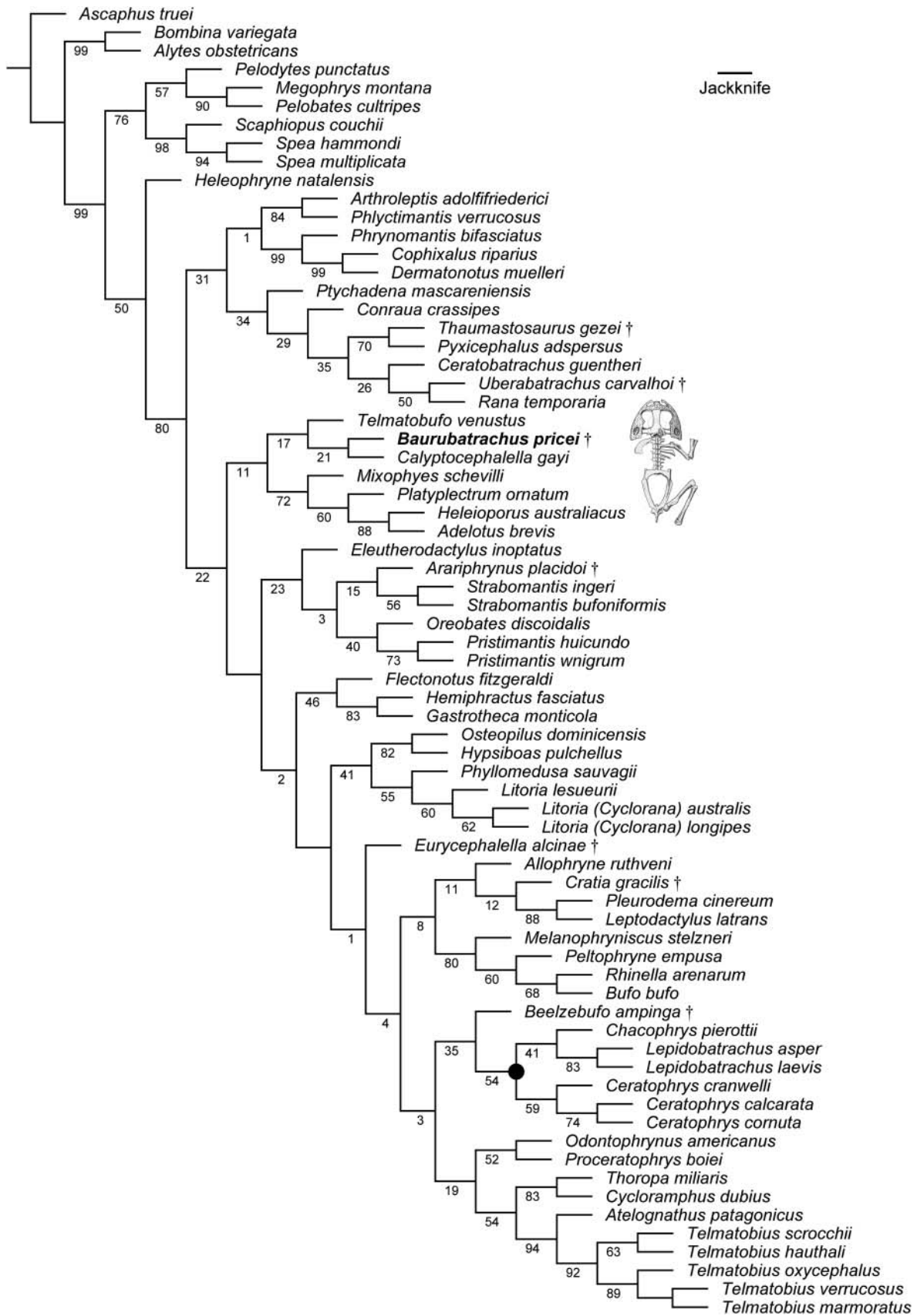
Figure 11. Tree retrieved in the parsimony analysis, with optimization of the full number of characters over a constrained topology based on the molecular phylogeny of Pyron & Wiens (2011); characters are considered equally weighted (length 1259 steps). Solid circle indicates crown-group Ceratophryidae.
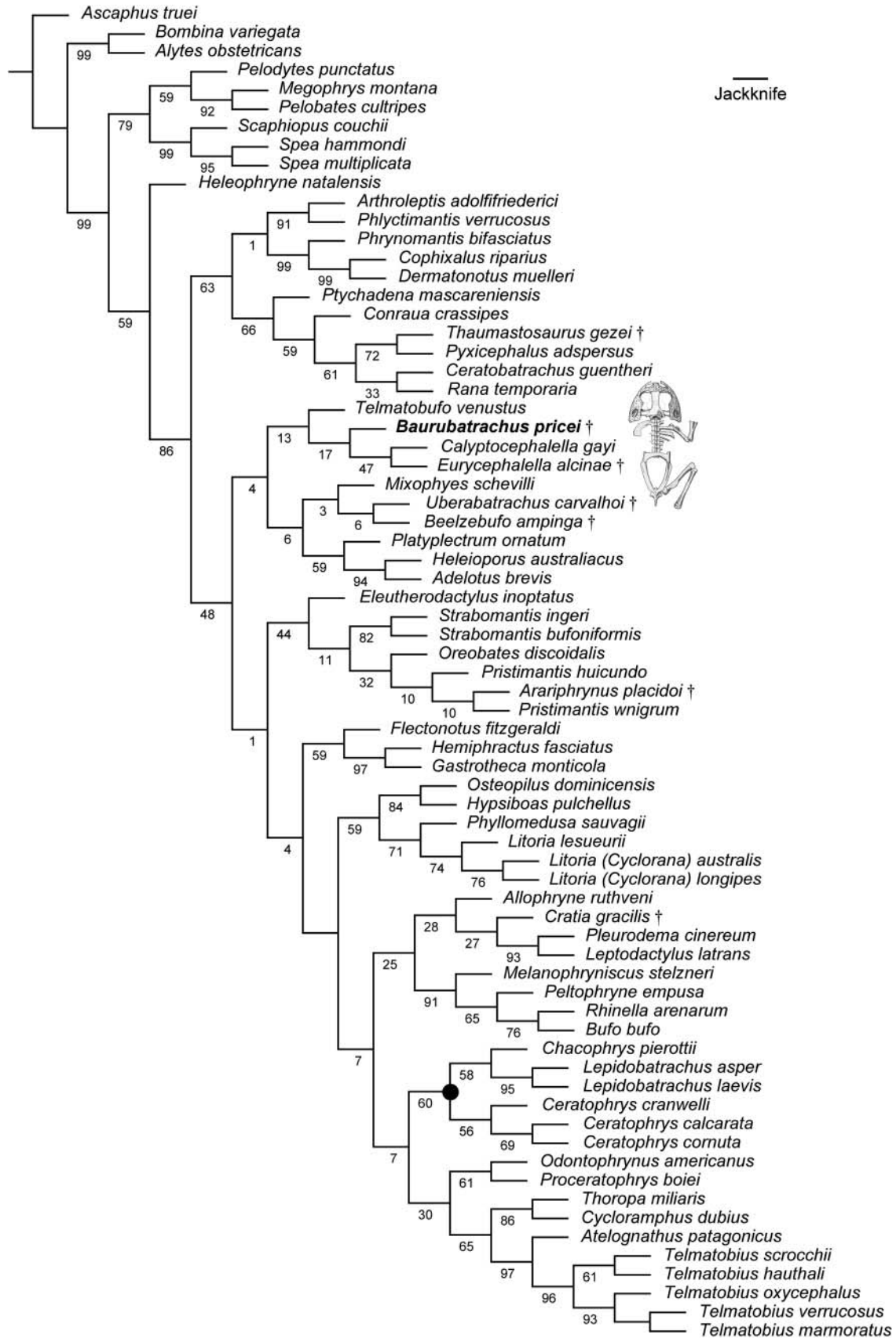
Figure 12. Tree retrieved in the parsimony analysis, with optimization of the full number of characters over a constrained topology based on the molecular phylogeny of Pyron & Wiens (2011) and Faivovich *et al.* (2014); characters are subjected to implied weighting using the concavity constant k = 7. Solid circle indicates crown-group Ceratophryidae.

two unambiguous synapomorphies (dorsal process of quadratojugal (54:1) and slightly expanded sacral diapophyses (86:2)), but the node including its sister taxon, *Beelzebufo*, is supported by six cranial features: frontoparietal supraorbital flange (6:1), squamosal zygomatic ramus articulated with maxilla (10:2), pterygoid medial ramus articulated with parasphenoid ala (14:2), premaxillary *pars palatina* with lingual process (46:4), dermal ornamentation of sculpture of maxillary *pars facialis* lying over *pars dentalis* (50:2), and maxillary *pars palatina* parallel to or investing the *pars facialis* in the anterior orbital region (52:2). In the topology resulting from this analysis the first two conditions, presence of supraorbital flange and pterygoid and parasphenoid extensive contact, convergently support the sister-group relationship of *Baurubatrachus* and *Calyptocephalella*, together with two character states that do not occur in *Beelzebufo*: the markedly posterior lower jaw articulation (61:2) and the high iliac dorsal crest (123:2). In addition, it is worth noting that *Baurubatrachus*, like *Calyptocephalella*, has the plesiomorphic condition of the maxillary *pars palatina* (52:0) unlike *Beelzebufo* in which a shelf-like *pars palatina* is absent.

When the characters are subjected to implied weighting (k = 7) the constrained analysis retrieves 20 synapomorphies for the ceratophryid node. These synapomorphies include the six cranial conditions aforementioned, although with *Beelzebufo* now placed among australobatrachians these cranial features are shared convergently with members of this group (character states 6:1; 10:2; 14:2; 46:4; 50:2; 52:2), and 11 putative derived cranial and postcranial features that also support the ceratophryid node in the unconstrained search of the full matrix (e.g. extensive squamosal otic plate on prootic (9:2), squamosal–nasal contact (11:1), cartilaginous roofing of the *cavum cranii* (36:4), monocuspid teeth (44:1), symphyseal ectopic ossifications (59:1), alary processes of hyoid absent (65:1), calcifications on hyoid plate (71:1), atlantal confluent cotyles (76:0), and long transverse processes on presacral IV (83:1)). In turn, the relationship of *Baurubatrachus* and *Calyptocephalella* (plus the mid-Cretaceous *Eurycephalella*) is supported by the same five synapomorphies supporting these two taxa retrieved in the constrained analysis under equal weights mentioned above.

Evans *et al.* (2014) listed 10 synapomorphies supporting the ceratophryid crown clade, which included *Beelzebufo* and *Baurubatrachus* as members in their study. Some of these ceratophryid synapomorphies are also recovered in our analyses, such as the absence of anterolateral processes of the hyoid (our character state 65:0) and monocuspid teeth (our character 44:1) but they are not documented in the available fossil materials. The femoral crest, another of their 10 putative ceratophryid synapomorphies, occurs in all ceratophryids examined and many other taxa of our dataset, whereas loss of the crest

optimizes as a synapomorphy of Ranoides in our molecular constrained analysis. It is also worth noting that the absence of contact between the vomer and the maxillary arch, listed as a ceratophryid synapomorphy by Evans *et al.* (2014), is probably in error because it is not a condition present in the living members of the clade. Codings of other characters differ from the present study.

Fabrezi & Quinzio (2008) also retrieved a monophyletic Ceratophryidae (Ceratophryinae therein) supported by 17 larval and adult morphological synapomorphies. However, these putative ceratophryid synapomorphies were retrieved in a small-scale morphology-based phylogenetic analysis performed with the aim of having a phylogenetic context to ultimately identify the heterochronic changes in the ontogeny of these frogs that might have shaped their body plans. In the maximum parsimony analysis of these authors (Fabrezi & Quinzio 2008), performed with TNT v.1.0 and rooted against *Bombina orientalis*, four extant ceratophryid species (*Ceratophrys cranwelli, Chacophrys pierottii, Lepidobatrachus laevis, L. llanensis,*) and six non-ceratophryid species, mostly moderately ossified taxa, were scored for 61 larval and 41 adult morphological characters. With the exception of *Discoglossus pictus* and *Pseudis platensis*, all these species or closely related species of the same genera were included in our present investigation. Also, all these adult morphological characters were considered in our analyses. The majority of the adult ceratophryid synapomorphies proposed by Fabrezi & Quinzio (2008) are osteological and many can be ascertained in the available material of *Baurubatrachus* (e.g. squamosal sutured to maxilla, lower jaw articulation posterior to the cranio-vertebral joint), whereas one of the four putative larval synapomorphies can be inferred from the condition in the only known specimen of this taxon (*tectum cavum cranii* almost completely chondrified). However, other osteological ceratophryid synapomorphies listed by Fabrezi & Quinzio (2008) cannot be assessed unambiguously in *Baurubatrachus* owing to the lack or poor preservation of the pertinent skeletal parts. This is the case for the fangs on the lower jaw, the mento-meckelian bone completely fused to dentary, the non-pedicellate teeth, the absence of anterolateral processes of the hyoid, and ossification of the posteromedial processes invading the hyoid plate. Conversely, a few ceratophryid synapomorphies from the list by Fabrezi & Quinzio (2008) are not present in *Baurubatrachus*, such as lack of the dorsal crest along the iliac shaft (although a distinct ridge may be present). In *Baurubatrachus*, the ilium unquestionably bears a distinct crest along the dorsal side of most of the shaft (Fig. 7), thus being unlike the supposedly derived, crestless iliac shaft of ceratophryids (Fabrezi *et al.* 2016). In addition, apart from the presence or absence of a dorsal crest, the ilium of *Baurubatrachus* is radically different from that of living ceratophryids in having an elongate dorsal protuberance on a dorsal

prominence that is confluent with the dorsal crest, and an acute angle between the shaft and the ventral acetabular expansion. The premaxilla lacking a well-developed lingually directed palatine shelf and having a posterolaterally directed expansion for an extended articulation with the maxilla were both considered derived features of ceratophrhyines by Fabrezi (2006) and Evans *et al.* (2008). The premaxillae of *Baurubatrachus* are missing and, therefore, we were unable to reconstruct the configuration of this element.

Which is the minimal placement of *Baurubatrachus* within Neobatrachia?

Our maximum parsimony analyses, performed to investigate the evolutionary relationships of *Baurubatrachus*, consistently place this taxon within Neobatrachia. Whether this speciose clade had its origin in Gondwana remains contentious (Roelants *et al.* 2007; Irisarri *et al.* 2012), whereas its early diversification was probably affected by the Mesozoic break up of this supercontinent (Frazao *et al.* 2015). Even though its phylogenetic position is not strongly supported in our analyses, *Baurubatrachus* is probably a hyloid relative rather than a ranoid. This placement is consistent with the molecular time estimates of the Ranoides/Hyloides split, although these estimates are widely divergent, covering a time span of 64 myr (Early Jurassic–Early Cretaceous), with a median at 159.6 Ma (Oxfordian, Late Jurassic) (Hedges *et al.* 2015). *Baurubatrachus* has one of the two synapomorphies that support the Hyloides node in our constrained analyses (under equal weights and with implied weighting, k = 7): ossified *crista parotica* (38:1). The other hyloid synapomorphy, presence of *tectum parietale* (36:3), is probably present in *Baurubatrachus* owing to the complete roofing of the *cavum cranii* in the preserved remains.

Among hyloids, *Baurubatrachus* clusters with members of the Gondwanan clade Australobatrachia, although with low support, sharing with them the distally expanded *crista parotica* (39:1). Although frequently retrieved associated with calyptocephalellids, we cannot rule out that this fossil might represent a stem-australobatrachian based on the available evidence. The palaeontological record documents that by the Campanian–Maastrichtian, calyptocephalellids not only had diverged from myobatrachoids, their sister group, but they were already common components of the northern Patagonian lacustrine and coastal lowland environments linked to the Atlantic Late Cretaceous–Danian transgression (Báez 1987; Martinelli & Forasiepi 2004; Gómez *et al.* 2011). Therefore, the divergence into the two main australobatrachian clades might have occurred no later than 79.5 Ma based on the estimated age of the strata that underlies the beds that yielded the calyptocephalellid remains (Dingus *et al.* 2000). Further, myobatrachoids have been recorded in the Lower Eocene of Australia (Tyler & Godthelp 1993), suggesting that by then their diversification in this continent was well underway.

We might explore whether *Baurubatrachus* is a nobleobatrachian. Molecular time estimates for the origin of the nobleobatrachian crown clade, sister group of Australobatrachia according to most phylogenetic analyses (Frost el al. 2006; Roelants *et al.* 2007; Pyron & Wiens 2011), are widely disparate, with a median of 70.9 Ma (Maastrichtian) (Hedges *et al.* 2015). In this regard, the earliest described fossils that probably represent crown nobleobatrachians are from Eocene rocks (e.g. Poinar & Cannatella 1987), setting aside the poorly preserved neobatrachians of ambiguous phylogenetic position from the mid-Cretaceous Crato Formation (Báez *et al.* 2009). In turn, molecular estimates for the diversification of Hyloides have a median of 134.6 Ma (Valanginian) (Hedges *et al.* 2015), thus implying a long branch leading to crown Nobleobatrachia with a duration of 63.7 myr, roughly equivalent to the entire Cainozoic. We were unable to retrieve any osteological synapomorphy for Nobleobatrachia, a node that lacks unambiguous morphological support to date (Frost *et al.* 2006). This hampers the placement of any fossil taxon, including *Baurubatrachus*, on its stem as well as knowledge of the evolution of characters in this branch and assessment of the putative synapomorphies of the sister lineage.

Is homoplasy blurring the results?

Homoplasy has been defined as similarity that is the result not of simple ancestry but of either reversal to an ancestral trait in a lineage or of independent evolution (Wake *et al.* 2011). A phylogenetic analysis is necessary to reveal whether the observed similarity is not simply inherited from the common ancestor of the taxa being compared; in turn, high levels of homoplasy, which increase with increasing number of taxa, constitute a major concern to phylogenetic reconstruction and may produce misleading results. Several approaches to attenuate the confounding effects of homoplasy in phylogenetics have been suggested, including the exclusion of taxa or characters that are suspected to be more homoplastic (e.g. Wiens *et al.* 2005) or weighting against homoplasy during character optimization on a tree (Farris 1969; Goloboff 1993). The first approach might be discouraged in some cases, since it relies on recognizing homoplasy *a priori* (Wiens *et al.* 2005). Although the second approach does not suffer from the same flaw, it might be ineffective in properly down-weighting homoplastic characters when they are overrepresented in the sample.

Testing the systematic position of *Baurubatrachus* within Anura served as an empirical example, since homoplasy is ubiquitous in this clade, particularly regarding features related to skeletal hyperossification (e.g.

Gómez *et al.* 2011) and the available information on fossil taxa is inherently limited. Our approach to dealing with homoplasy in this particular case, which combined some previous proposals that are in line with the principle of total evidence (e.g. Kluge 1989), can be summarized as follows. We included a broad taxonomic sample, so that alternative hypotheses are testable, and considered as many distantly related taxa (based on other lines of evidence) that share features that may have evolved homoplastically as possible. We included taxa with well-ossified dermatocrania as well as less-ossified close relatives. We considered characters from as many different parts of the system under study as possible, to diminish the impact of suspected homoplastic features from a single structural part (e.g. the skull), which might be prone to being correlated. We analysed the impact of presumed homoplastic characters by excluding them from the analysis, yet it is noteworthy that they carry useful phylogenetic information at different hierarchical levels and so they are worth of inclusion. Also, we selected a phylogram of the taxa under study based on molecular sequence data, which served as a scaffold to explore the position of *Baurubatrachus* and the evolution of characters under this assumption. In this way we confirmed, for instance, that a supraorbital flange and a maxilla-squamosal articulation are derived traits that developed homoplastically in *Calyptocephalella* and the ceratophryids. Additionally, we searched for optimal topologies under implied weighting to downweight supposed homoplasy. These actions do not warrant the total avoidance of the misleading effects of homoplasy, but they are one way to prepare for the worst and hope for the best.

Microhabitat and habits of *Baurubatrachus*

The sedimentary successions that constitute the Marilia Formation are continental volcaniclastic deposits formed in braided fluvial systems, alluvial fans and ephemeral lakes mainly distributed in the intracontinental depression of the Bauru Basin (Fernandes & Coimbra 2000). At the time the climate was seasonal and long, dry intervals were interrupted periodically by rains that flooded the small lakes and temporary ponds. The first rains were probably torrential, killing many of the diverse animals that inhabited the region and suddenly transporting and burying them under large quantities of sediment (Vasconcellos & Carvalho 2006).

The preserved overall anatomy of *Baurubatrachus* does not include obvious specializations usually related to certain particular locomotor modes and other behaviours associated with the use of the substrate, such as long-distance jumping, climbing, or digging. The known limb proportions are rather generalized and consistent with a ground dwelling and/or aquatic (but not a specialized swimmer) frog (Lires *et al.* 2016). These proportions, together with the crested ilium,

speak against a fossorial existence but are compatible with some burrowing activity to avoid desiccation in the water-bodies during the dry season. When features of the skull are considered, other behavioural issues emerge. The exostosic, relatively large but depressed skull with markedly posterior cranio-mandibular joints presently occur in few non-obligate aquatic anurans that forage for large prey in water, such as the australobatrachian *Calyptocephalella gayi* (Muzzopappa *et al.* 2016) and the ceratophryids of the genus *Lepidobatrachus* (Fabrezi 2006). Although extant representatives of these taxa lack the dorsal exposure of the *crista parotica* present in *Baurubatrachus*, it is noteworthy that extinct relatives of *C. gayi* lack a full contact between the *lamella alaris* of the squamosal and the frontoparietal (Gómez *et al.* 2011). The posterior position of the lower jaw articulation has been considered mechanically advantageous for feeding on large and slow prey, together with the development of adductor musculature to ensure a rapid and strong closure (Emerson 1985). The well-developed coronoid process and the ventral flange of the pterygoid in *Baurubatrachus* are consistent with having powerful adductor muscles. These features suggest this Cretaceous species might have captured the prey in the same way as those living taxa, which also make use of their forelimbs to scoop the prey towards the mouth (O'Reilly *et al.* 2002). In this regard, the actions of the *scapularis* portion of the deltoid muscle in *Baurubatrachus* mentioned above lend support to this hypothesis. The presence of round openings encircled by ornamented bone in the skull roof of *Baurubatrachus* is an extremely rare feature amongst living anurans but its biological meaning has not been studied. The intense dermal ossification of this region in *Baurubatrachus* might be related to the stress produced by muscular action such as that of the *sternocleidomastoideus*.

Conclusions

Preparation of the type and only known specimen of the bizarre neobatrachian frog *Baurubatrachus pricei* from the Maastrichtian of Brazil revealed new significant data, allowing detailed osteological description of its anatomy. Of particular interest are the morphologies of elements of the pectoral and pelvic girdles, which are at odds with the ceratophryid affinities that were previously proposed for this extinct taxon. Novel phylogenetic analyses under various conditions of character weighting, character partitions, and topological constraints, although consistently recovering a robust monophyletic Ceratophryidae, refute this hypothesis. Further examination of the results highlights the homoplastic nature of several cranial features presumably linked to dermal hyperossification, stressing the problem of leaning too heavily on these kinds of characters.

In our analyses *Baurubatrachus* is repeatedly recovered as a member of Neobatrachia and clustered with hyloid

taxa, as a close relative of the living australobatrachian helmeted frog *Calyptocephalella gayi*, sharing not only features of the hyperossified skull but also several postcranial traits. It is noteworthy that our analyses using a molecular scaffold tree also recovered most other Gondwanan Cretaceous neobatrachians in relatively basal positions among hyloids, either as australobatrachians or basal nobleobatrachians. However, we must be cautious and consider that Nobleobatrachia still lacks morphological synapomorphies and a position of *Baurubatrachus* or other fossil taxa on the stems of these two large hyloid clades cannot be completely ruled out.

Acknowledgements

Supplemental material

Supplemental material for this article can be accessed at: http://dx.doi.org/10.1080/14772019.2017.1287130

References

Agnolin, F. 2012. A new Calyptocephalellidae (Anura, Neobatrachia) from the Upper Cretaceous of Patagonia, Argentina, with comments on its systematic position. *Studia geologica salmanticensia*, **48**, 129–178.

Báez, A. M. 1985. Anuro leptodactílido en el Cretácico Superior (Grupo Bauru) de Brasil. *Ameghiniana*, **22**, 75–79.

Báez, A. M. 1987. The Late Cretaceous fauna of Los Alamitos, Patagonia, Argentina. III: Anurans. *Revista Museo Argentino de Ciencias Naturales*, **3**, 121–130.

Báez, A. M. & **Gómez, R. O.** 2014. Is hyperossification concealing the phylogenetic signal of osteological traits in anurans?

A test-case from the Upper Cretaceous of Brazil. *Society of Vertebrate Paleontology, 74th Annual Meeting, Berlin, Germany, Meeting Program and Abstracts*, p. 83.

Báez, A. M. & **Perí, S.** 1989. *Baurubatrachus pricei*, nov. gen. et sp., un anuro del Cretácico Superior de Minas Gerais, Brasil. *Anais da Academia Brasileira de Ciências*, **61**, 447–458.

Báez, A. M. & **Perí, S.** 1990. Revisión de *Wawelia gerholdi*, un anuro del Mioceno de Patagonia. *Ameghiniana*, **27**, 379–386.

Báez, A. M., **Muzzopappa, P.** & **Nicoli, L.** 2005. The Late Cretaceous neobatrachian frog *Baurubatrachus* revisited. *II Congreso Latinoamericano de Paleontología de Vertebrados. Museu Nacional, Río de Janeiro, Brasil, Boletim de resumos*, 45–46.

Báez, A. M., **Moura, G. J. B.** & **Gómez, R. O.** 2009. Anurans from the Lower Cretaceous Crato Formation of northeastern Brazil: implications for the early divergence of neobatrachians. *Cretaceous Research*, **30**, 829–846.

Báez, A. M., **Gómez, R. O.** & **Taglioretti, M. L.** 2012. The archaic ilial morphology of an enigmatic pipid frog from the upper Pleistocene of the South American pampas. *Journal of Vertebrate Paleontology*, **32**, 304–314.

Barbour, T. 1914. A contribution to the zoogeography of the West Indies, with especial reference to amphibians and reptiles. *Memoirs of the Museum of Comparative Zoology*, **44**, 2209–2346.

Barbour, T. 1926. *Reptiles and amphibians. Their habits and adaptations*. The Riverside Press, Cambridge, MA, 125 pp.

Blotto, B. L., **Nuñez, J. J.**, **Basso, N. G.**, **Ubeda, C. A.**, **Wheeler, W. C.** & **Faivovich, J.** 2013. Phylogenetic relationships of a Patagonian frog radiation, the *Alsodes + Eupsophus* clade (Anura: Alsodidae), with comments on the supposed paraphyly of *Eupsophus*. *Cladistics*, **29**, 113–131.

Bolkay, S. J. 1919. Osnove uporedne osteologije anurskih batrahija sa dodatkom o porijeklu Anura i sa slikom naravnoga sistema istih. *Glasnik Zemaljskog Muzeja Bosni Hercegovini*, **31**, 277–353.

Cannatella, D. C. & **Trueb, L.** 1988. Evolution of pipoid frogs: intergeneric relationships of the aquatic frog family Pipidae (Anura). *Zoological Journal of the Linnean Society*, **94**, 1–38.

Darda, D. M. & **Wake, D. B.** 2015. Osteological variation among extreme morphological forms in the Mexican salamander Genus *Chiropterotriton* (Amphibia: Plethodontidae): Morphological Evolution and Homoplasy. *PLoS ONE*, **10** (6), e0127248.

De la Riva, I., **Trueb, L.** & **Duellman, W.** 2012. A new species of *Telmatobius* (Anura: Telmatobiidae) from montane forests of southern Peru, with a review of osteological features of the genus. *South American Journal of Herpetology*, **7**, 91–109.

Dingus, L., **Clarke, J.**, **Scott, G. R.**, **Swisher III, C. C.**, **Chiappe, L. M.** & **Coria, R. A.** 2000. Stratigraphy and magnetostratigraphic/faunal constraints for the age of sauropod embryo-bearing rocks in the Neuquén Group (Late Cretaceous, Neuquén Province, Argentina). *American Museum Novitates*, **3290**, 1–11.

Ecker, A. 1889. *The anatomy of the frog. Translations of foreign biological memoirs 2*. Clarendon Press, Oxford, 460 pp.

Emerson, S. B. 1976. Burrowing in frogs. *Journal of Morphology*, **149**, 437–458.

Emerson, S. B. 1985. Skull shape in frogs: correlations with diet. *Herpetologica*, **41**, 177–188.

Evans, S. E., **Jones, M. E. H.** & **Krause, D. W.** 2008. A giant frog with South American affinities from the Late Cretaceous of Madagascar. *Proceedings of the National Academy of Sciences of the United States of America*, **105**, 2951–2956.

Evans, S. E., **Groenke, J. R.**, **Jones, M. E. H.**, **Turner, A. H.** & **Krause, D. W.** 2014. New material of *Beelzebufo*, a hyperossified frog (Amphibia, Anura) from the Late Cretaceous of Madagascar. *PLoS ONE*, **9** (1), e87236.

Fabrezi, M. 1992. El carpo de los anuros. *Alytes*, **10**, 1–29.

Fabrezi, M. 1993. The anuran tarsus. *Alytes*, **11**, 47–63.

Fabrezi, M. 2006. Morphological evolution of the Ceratophryinae (Anura, Neobatrachia). *Journal of Zoological Systematics and Evolutionary Research*, **44**, 153–166.

Fabrezi, M. & **Alberch, P.** 1996. The carpal elements of anurans. *Herpetologica*, **52**, 188–204.

Fabrezi, M. & **Quinzio, S. I.** 2008. Morphological evolution in Ceratophryinae frogs (Anura: Neobatrachia): the effect of heterochronic changes during larval development and metamorphosis. *Zoological Journal of the Linnean Society*, **154**, 752–780.

Fabrezi, M., **Quinzio, S. I.**, **Goldberg, J.**, **Cruz, J. C.**, **Chuliver Pereyra, M.** & **Wassersug, R. J.** 2016. Developmental changes and novelties in ceratophryid frogs. *EvoDevo*, **7**, doi: 10.1186/s13227-016-0043-9.

Faivovich, J., **Nicoli, L.**, **Blotto, B. L.**, **Pereira, M. O.**, **Baldo, D.**, **Barrionuevo, J. S.**, **Fabrezi, M.**, **Wild, E.** & **Haddad, C. F. B.** 2014. Big, bad, and beautiful: phylogenetic relationships of the horned frogs (Anura, Ceratophryidae). *South American Journal of Herpetology*, **9**, 207–227.

Farris, J. S. 1969. A successive approximations approach to character weighting. *Systematic Biology*, **18**, 374–385.

Fernandes, L. A. 2010. Calcretes e registros de paleossolos em depósitos continentais neocretáceos (Bacia Bauru, Formação Marília). *Revista Brasileira de Geociências*, **40**, 19–35.

Fernandes, L. A. & **Coimbra, A. M.** 2000. Revisão estratigráfica da parte oriental da Bacia Bauru (Neocretaceo). *Revista Brasileira de Geociências*, **30**, 717–728.

Fischer von Waldheim, G. 1813. *Zoognosia tabulis synopticis illustrata, in usum prælectionum Academiæ Imperialis Medico-Chirurgicæ Mosquensis edita. 3rd edition, Volume 1.* Nicolai Sergeidis Vsevolozsky, Moscow.

Frazao, A., **Silva, H. R. d.** & **Russo, C. A. d. M.** 2015. The Gondwana breakup and the history of the Atlantic and Indian Oceans unweils two new clades for early neobatrachian diversification. *PLoS ONE*, **10** (11), e0143926.

Frost, D. R. 2014. *Amphibian species of the world: an online reference*. Vers. 6.0 (30 July 2014). Electronic database accessible at: http://research.amnh.org/herpetology/amphibia/index.plp. American Museum of Natural History, New York.

Frost, D. R., **Grant, T.**, **Faivovich, J.**, **Bain, R. H.**, **Haas, A.**, **Haddad, C. F. B.**, **De Sá, R. O. D.**, **Channing, A.**, **Wilkinson, M.**, **Donnellan, S. C.**, **Raxworthy, C. J.**, **Campbell, J. A.**, **Blotto, B. L.**, **Moler, P.**, **Drewes, R. C.**, **Nussbaum, R. A.**, **Lynch, J. D.**, **Green, D. M.** & **Wheeler, W. C.** 2006. The amphibian tree of life. *Bulletin of the American Museum of Natural History*, **297**, 1–370.

Goldberg, K. & **Garcia, A. J. V.** 2000. Paleobiogeography of the Bauru Group, a dinosaur-bearing Cretaceous unit, northeastern Parana Basin, Brazil. *Cretaceous Research*, **21**, 241–254.

Goloboff, P. A. 1993. Estimating character weights during tree search. *Cladistics*, **9**, 83–91.

Goloboff, P., **Farris, J.** & **Nixon, K.** 2008. TNT, a free program for phylogenetic analysis. *Cladistics*, **24**, 774–786.

Gómez, R. O. & **Turazzini, G. F.** 2016. An overview of the ilium of anurans (Lissamphibia, Salientia), with a critical appraisal of the terminology and primary homology of main ilial features. *Journal of Vertebrate Paleontology*, **36**, e1030023.

Gómez, R. O., **Báez, A. M.** & **Muzzopappa, P.** 2011. A new helmeted frog (Anura: Calyptocephalellidae) from an Eocene subtropical lake in northwestern Patagonia, Argentina. *Journal of Vertebrate Paleontology*, **31**, 50–59.

Gomez-Mestre, I., **Pyron, R. A.** & **Wiens, J. J.** 2012. Phylogenetic analyses reveal unexpected patterns in the evolution of reproductive modes in frogs. *Evolution*, **66**, 3687–3700.

Griffiths, I. 1959. The phylogenetic status of the Sooglossidae. *Annals and Magazine of Natural History*, **2**, 626–640.

Haas, A. 2003. Phylogeny of frogs as inferred from primarily larval characters (Amphibia: Anura). *Cladistics*, **19**, 23–90.

Hedges, S. B., **Marin, J.**, **Suleski, M.**, **Paymer, M.** & **Kumar, S.** 2015. Tree of life reveals clock-like speciation and diversification. *Molecular Biology and Evolution*, **32**, 835–845.

Henrici, A., **Báez, A. M.** & **Grande, L.** 2013. *Aerugoamnis paulus*, new genus and new species (Anura: Anomocoela): first reported anuran from the early Eocene (Wasatchian) Fossil Butte member of the Green River Formation, Wyoming. *Annals of the Carnegie Museum*, **81**, 295–309.

Irisarri, I., **San Mauro, D.**, **Abascal, F.**, **Ohler, A.**, **Vences, M.** & **Zardoya, R.** 2012. The origin of modern frogs (Neobatrachia) was accompanied by acceleration in mitochondrial and nuclear substitution rates. *BMC Genomics*, **13**, doi: 10.1186/1471-2164-13-626.

Jared, C., **Antoniazzi, M. M.**, **Katchburian, E.**, **Toledo, R. C.** & **Freidmüller, E.** 1999. Some aspects of the natural history of the casque-headed tree frog *Corythomantis greeningi* Boulenger (Hylidae). *Annales des Sciences Naturelles*, **3**, 105–115.

Kluge, A. G. 1989. A concern for evidence and a phylogenetic hypothesis of relationships among *Epicrates* (Boidae, Serpentes). *Systematic Biology*, **38**, 7–25.

Laloy, F., **Rage, J-C.**, **Evans, S. E.**, **Boistel, R.**, **Lenoir, N.** & **Laurin, M.** 2013. A re-interpretation of the Eocene anuran *Thaumastosaurus* based on microCT examination of a 'mummified' specimen. *PLoS ONE*, **8**(9), e74874.

Laurent, R. 1943. Note sur l'ostéologie de deux Ranides exotiques. *Bulletin du Museé Royal d'Histoire naturelle de Belgique*, 19(27), 1–4.

Lires, A. I., **Soto, I. M.** & **Gómez, R. O.** 2016. Walk before you jump: new insights on early frog locomotion from the oldest known salientian. *Paleobiology*, **42**, 612–623.

Lynch, J. D. 1971. Evolutionary relationships, osteology and zoogeography of leptodactyloid frogs. *Miscellaneous Publication*, *Museum of Natural History, University of Kansas*, **53**, 1–238.

Lynch, J. D. 1973. The transition from archaic to advanced frogs. Pp. 133–182 in J. L. Vial (ed.) *Evolutionary biology of the anurans. Contemporary research on major problems*. University of Missouri Press, Columbia.

Lynch, J. D. 1975. A review of the broad-headed eleutherodactyline frogs of South America (Leptodactylidae). *Occasional Papers of the Museum of Natural History*, *The University of Kansas, Lawrence, Kansas*, **38**, 1–46.

Lynch, J. D. 1982. Relationships of the frogs of the genus *Ceratophrys*(Leptodactylidae) and their bearing on hypotheses of Pleistocene forest refugia in South America and punctuated equilibria. *Systematic Zoology*, **31**, 166–179.

Martinelli, A. G. & **Forasiepi, A.** 2004. Late Cretaceous vertebrates from Bajo de Santa Rosa (Allen Formation), Rio Negro province, Argentina, with the description of a new sauropod dinosaur (Titanosauridae). *Revista del Museo Argentino de Ciencias Naturales, Nueva Serie*, **6**, 257–305.

Moen, D. S., **Irschick, D. J.** & **Wiens, J. J.** 2013. Evolutionary conservatism and convergence both lead to striking similarity in ecology, morphology and performance across continents in frogs. *Proceedings of the Royal Society, Biological Series*, **280**, 20132156.

Moen, D. S., **Morlon, H.** & **Wiens, J. J.** 2016. Testing convergence versus history: convergence dominates phenotypic evolution for over 150 million years in frogs. *Systematic Biology*, **65**, 161–176.

Muzzopappa, P., **Pugener, A.** & **Báez, A. M.** 2016. Postcranial osteogenesis of the helmeted water toad *Calyptocephalella gayi* (Neobatrachia: Calyptocephalellidae) with comments on the osteology of australobatrachians. *Journal of Morphology*, **277**, 204–230.

Nicoli, L., **Muzzopappa, P.** & **Faivovich, J.** 2016. The taxonomic placement of the Miocene Patagonian frog *Wawelia gerholdi* (Amphibia: Anura). *Alcheringa: An Australasian Journal of Palaeontology*, **40**, 153–160.

O'Reilly, J. C., **Deban, S. M.** & **Nishikawa K. C.** 2002. Derived life history characteristics constrain the evolution of aquatic feeding behavior in adult amphibians. Pp. 153–190 in P. Aerts, K. D'Août, A. Herrel & J. Van Damme (eds) *Topics in functional and ecological vertebrate morphology*. Shaker Publishing, Maastricht.

Poinar Jr, G. O. & **Cannatella, D. C.** 1987. An Upper Eocene frog from the Dominican Republic and its implication for Caribbean biogeography. *Science*, **237**, 1215–1216.

Pramuk, J. B. 2002. Combined evidence and cladistic relationships of West Indian toads (Anura: Bufonidae). *Herpetological Monographs*, **16**, 121–151.

Pregill, G. 1981. Cranial morphology and the evolution of West Indian toads (Salientia: Bufonidae): resurrection of the genus *Peltophryne* Fitzinger. *Copeia*, **1981**, 273–285.

Pyron, R. A. & **Wiens, J. J.** 2011. A large-scale phylogeny of Amphibia including over 2800 species, and a revised classification of extant frogs, salamanders, and caecilians. *Molecular Phylogenetics and Evolution*, **61**, 543–583.

Reig, O. A. 1958. Proposiciones para una nueva macrosistemática de los anuros (nota preliminar). *Physis*, **21**, 109–118.

Reig, O. A. 1960. Las relaciones genéricas del anuro chileno Calyptocephalella gayi (Dum. & Bibr.). *Actas y Trabajos del Primer Congreso Sudamericano de Zoología, La Plata, Argentina*, **4**, 113–131.

Reinbach, W. 1939. Untersuchungen über die Entwicklung des Kopfskeletts von *Calyptocephalus* Gayi (mit einem Anhang über das Os supratemporale der anuren Amphibien). *Jenaische Zeitschrift für Naturwissenschaft*, **72**, 211–362.

Roček, Z. 2003. Larval development and evolutionary origin of the anuran skull. Pp. 1878–1995 in H. Heatwole & M. Davies (eds) *Amphibian Biology 5*. Surrey Beatty and Sons, Chipping Norton, New South Wales.

Rodriguez Talavera, **M. R.** 1990. *Evolución de pelobátidos y pelodítidos (Amphibia, Anura): Morfología y Desarrollo del Sistema Esquelético*. Doctoral thesis, Universidad Complutense de Madrid, 282 pp.

Roelants, K., **Gower, D. J.**, **Wilkinson, M.**, **Loader, S. P.**, **Biju, S. D.**, **Guillaume, K.**, **Moriau, L.** & **Bossuyt, F.** 2007. Global patterns of diversification in the history of modern amphibians. *Proceedings of the National Academy of Sciences of the United States of America*, **104**, 887–892.

Ruane, S., **Pyron, R. A.** & **Burbrink, F. T.** 2011. Phylogenetic relationships of the Cretaceous frog *Beelzebufo* from Madagascar and the placement of fossil constraints based on temporal and phylogenetic evidence. *Journal of Evolutionary Biology*, **24**, 274–285.

Scott, E. 2005. A phylogeny of ranid frogs (Anura: Ranoidea: Ranidae), based on a simultaneous analysis of morphological and molecular data. *Cladistics*, **21**, 507–574.

Sereno, P. 2007. Logical basis for morphological characters in phylogenetics. *Cladistics*, **23**, 565–587.

Sheil, C. & **Mendelson, J. R., III** 2001. A new species of *Hemiphractus* (Anura: Hylidae: Hemiphractinae), and a redescription of *H. johnsoni*. *Herpetologica*, **57**, 189–202.

Sigurdsen, T., **Green, D. M.** & **Bishop, P. J.** 2012. Did *Triadobatrachus* jump? Morphology and evolution of the anuran forelimb in relation to locomotion in early salientians. *Fieldiana Life and Earth Sciences*, **5**, 77–89.

Smith, S. A., **Nieto Montes de Oca, A.**, **Reeder, T. W.** & **Wiens, J. J.** 2007. A phylogenetics perspective on elevational species richness patterns in Middle-America tree frogs: in lowland tropical rainforests. Why so few species? *Evolution*, **61**, 1188–1207.

Trueb, L. 1973. Bones, frogs and evolution. Pp. 65–132 in J. L Vial (ed.) *Evolutionary Biology of the Anurans. Contemporary Research on Major Problems*. University of Missouri Press, Columbia.

Trueb, L. 1974. Systematic relationships of Neotropical horned frogs genus *Hemiphractus* (Anura, Hylidae). *Occasional Papers of the Museum of Natural History*, *University of Kansas*, **29**, 1–60.

Trueb, L. 1993. Patterns in cranial diversity among the Lissamphibia. Pp. 255–343 in J. Hanken & B. K. Hall (eds) *The vertebrate skull: patterns of structural and systematic diversity. Volume 2*. University of Chicago Press, Chicago.

Tyler, M. J. & **Godthelp, H.** 1993. A new species of *Lechriodus* Boulenger (Anura: Leptodactylidae) from the Early Eocene of Queensland. *Transactions of the Royal Society of Southern Australia*, **117**, 187–189.

Vasconcellos, F. M & **Carvalho, I. S.** 2006. Condicionante etológico na tafonomia de *Uberabasuchus terrificus* (Crocodyliformes, Peirosauridae) da Bacia Bauru (Cretáceo Superior). *Geociências*, **25**, 225–230.

Wake, D. B., **Wake, M. H.** & **Specht, C. D.** 2011. Homoplasy: from detecting pattern to determining process and mechanism of evolution. *Science*, **331**, 1032–1035.

Wake, D. B., **Blackburn, D. C.** & **Lombard, R. E.** 2015. Rampant homoplasy in complex characters: repetitive convergent evolution of amphibian feeding structures. Pp. 395–406 in K. P. Dial, N. Shubin & E. L. Brainerd (eds) *Great transformations in vertebrate evolution*. University of Chicago Press, Chicago.

Wild, E. R. 1997. Description of the adult skeleton and developmental osteology of the hyperossified horned frog *Ceratophrys cornuta* (Anura: Leptodactylidae). *Journal of Morphology*, **232**, 169–206.

Wild, E. R. 1999. Description of the chondrocranium and osteogenesis of the Chacoan burrowing frog, *Chacophrys pierotti* (Anura: Leptodactylidae). *Journal of Morphology*, **242**, 229–246.

Wiens, J. J. 1989. Ontogeny of the skeleton of *Spea bombifrons* (Anura: Pelobatidae). *Journal of Morphology*, **202**, 29–51.

Wiens, J. J., **Bonett, R. M.** & **Chippindale, P. T.** 2005. Ontogeny discombobulates phylogeny: paedomorphosis and higher-level salamander relationships. *Systematic Biology*, **54**, 91–110.

Zhang, P., **Liang, D.**, **Mao, R.-L.**, **Hillis, D. M.**, **Wake, D. B.** & **Cannatella, D. C.** 2013. Efficient sequencing of anurans mtDNAs and a mitogenomic exploration of the phylogeny and evolution of frogs. *Molecular Biology and Evolution*, **30**, 1899–1915.

Zweifel, R. G. 1971. Results of the Archbold Expeditions. No. 96. Relationships and distribution of *Genyophryne thomsoni*, a microhylid frog of New Guinea. *American Museum Novitates*, **2469**, 1–13.